High-resolution optical spectroscopy, magnetic properties, and single-crystal neutron diffraction of multiferroic $HoFe_3(BO_3)_4$: Magnetic structure

M. N. Popova,[1,*] E. P. Chukalina,[1] D. A. Erofeev,[1] I. A. Gudim,[2] I. V. Golosovsky,[3] A. Gukasov,[4] A. A. Mukhin,[5] and B. Z. Malkin[6]

[1]*Institute of Spectroscopy, Russian Academy of Sciences, 108840 Moscow, Troitsk, Russia*
[2]*L. V. Kirensky Institute of Physics, Siberian Branch of RAS, 660036 Krasnoyarsk, Russia*
[3]*National Research Center "Kurchatov Institute", B.P. Konstantinov Petersburg Nuclear Physics Institute, 188300 Gatchina, Russia*
[4]*Laboratoire Léon Brillouin, CEA-CNRS, CE-Saclay, 91191 Gif-sur-Yvette, France*
[5]*Prokhorov General Physics Institute, RAS, 119991 Moscow, Russia*
[6]*Kazan Federal University, 420008 Kazan, Russia*

(Received 25 September 2020; revised 3 January 2021; accepted 8 February 2021; published 5 March 2021)

The magnetic structure is usually determined by the neutron diffraction measurements. However, in the case of complex multisublattice magnetics, this method fails to give an unambiguous result. Here, on the example of multiferroic $HoFe_3(BO_3)_4$, we show that in the case of rare-earth (RE) compounds the right magnetic structure can be determined by additionally using optical spectroscopy and a theoretical analysis based on spectroscopic data. $HoFe_3(BO_3)_4$ demonstrates a series of phase transitions and interesting magnetic and magnetoelectric properties. The available information on the magnetic structure of the compound, necessary for understanding and utilizing these properties, is contradictory. To resolve the existing ambiguities, we apply a combined approach. The high-resolution spectroscopy data deliver a set of the Ho^{3+} crystal-field (CF) levels in the paramagnetic and both *easy-plane* and *easy-axis* magnetic phases. These data are used to determine CF and Ho^{3+}-Fe^{3+} exchange parameters and, then, to calculate the temperature dependencies of the magnetic susceptibility tensor of $HoFe_3(BO_3)_4$. Based on these calculations, we suggest an *easy-plane* antiferromagnetic structure with a collinear arrangement of the Fe spins along the *a* axis and induced noncolinear moments of magnetically nonequivalent Ho ions. The suggested structure is further confirmed by single-crystal elastic neutron scattering experiments. We argue that specific features of the magnetic properties of RE iron borates isostructural to $HoFe_3(BO_3)_4$ are governed by the energy patterns and the symmetry properties of the wave functions of the lower CF levels of the RE ground multiplet in the crystal field of the C_2 symmetry.

DOI: 10.1103/PhysRevB.103.094411

I. INTRODUCTION

Multiferroic materials with magnetic and electric polarization order attract considerable attention, especially in systems where polarization is induced by magnetic ordering [1–5]. Among them, a new interesting family of multiferroics, the rare-earth (RE) iron borates $REFe_3(BO_3)_4$ [6], exhibit a strong correlation of magnetic, electric, and optical properties due to exchange interactions between the iron and RE magnetic subsystems. Therefore, knowledge of the magnetic order is crucial for understanding their physical properties.

Neutron diffraction is a powerful tool for determining the magnetic order (see, e.g., Refs. [7,8]). But there are certain limitations in the case of complicated magnetic structures. It is not easy to distinguish between different structures, which give close goodness-of-fit convergence parameters. In this case, the analysis of neutron scattering data should be combined with bulk magnetic, thermodynamic, and other methods (see, e.g., Refs. [9–11]). This is just the case of the magnetic structure of the multiferroic iron borate $HoFe_3(BO_3)_4$, where controversial data exist. To solve this problem, we combine theoretical considerations based on the high-resolution optical spectroscopy results with the measurements and analysis of single-crystal elastic neutron scattering data. It should be noted that the importance of combined studies of inelastic neutron scattering and optical spectra in order to determine the crystal-field levels of RE ions and exchange splitting of levels was emphasized in Ref. [12].

Holmium iron borate $HoFe_3(BO_3)_4$ crystallizes in the structure of the natural mineral huntite with the $R32$ space group [13,14]. At a temperature of about 360 K, the compound undergoes a first-order phase transition to a less symmetric structure with the $P3_121$ space group. In this structure, the symmetry of the RE site lowers from D_3 to C_2, its threefold C_3 axis disappears, and only one of the three C_2 axes survives. Instead of all equivalent Fe atoms, there are two different sites, Fe1 and Fe2 [14].

Anisotropy of the RE^{3+} ion promotes either an easy-axis (RE = Pr, Tb, Dy) or an easy-plane (RE = Nd, Sm, Er, Y) type of magnetic structure of $REFe_3(BO_3)_4$ below the Néel temperature $T_N \sim 30$–40 K [15]. $HoFe_3(BO_3)_4$ orders antiferromagnetically at $T_N = 38.5$ K into a structure of the *easy-plane* type [16–18], with Fe spins in the basal plane, perpendicular to the trigonal axis. However, competition between magnetic anisotropies of the iron and holmium subsystems

*Corresponding author: popova@isan.troitsk.ru

(of the easy-plane type and the temperature-dependent easy-axis type, respectively) leads to a first-order spin-reorientation phase transition at $T_{SR} \approx 5$ K into an antiferromagnetic structure of the *easy-axis* type [16,18,19]. All three phase transitions of $HoFe_3(BO_3)_4$ were detected by different methods, including the high-resolution optical spectroscopy [20].

Based on the powder neutron diffraction experiments [18], the magnetic peaks were indexed with a magnetic propagation vector $k = [0\ 0\ 1/2]$ corresponding to a magnetic unit cell doubled in the hexagonal c direction. At 2 K, an *easy-axis* magnetic structure of Fe spins was found in Ref. [18], with the antiferromagnetic coupling along the c direction and ferromagnetic arrangement in the ab plane. According to Ref. [18], the magnetic moments of the Fe ions are aligned along the c axis, while the Ho moments have the components not only along the c axis but also within the ab plane. At the translation $c/3$, the Fe and Ho components along the c axis change direction, while the in-plane components of Ho moments rotate by the angle 120 °. Above the spin-reorientation transition at about 5 K, an *easy-plane* magnetic structure reported in Ref. [18] possesses a noticeable nonzero out-of-plane component of the iron magnetic moments at the Fe2 sites. Moments at the Fe1 sites and the Ho moments are lying exclusively in the basal plane. However, a physical mechanism responsible for the out-of-plane components of the Fe spins remained unknown. The resonant and nonresonant x-ray scattering studies performed in Ref. [21] revealed a different, "screw type," magnetic structure of the induced Ho moments within the ab plane and along the c axis. This could indicate a significant role of the local magnetic anisotropy of the Ho^{3+} ions in the low-symmetry sites (C_2), which was neglected in Ref. [18].

To clarify these questions, we performed a comprehensive study of $HoFe_3(BO_3)_4$ by different methods. First, we measured and analyzed the high-resolution broadband polarized optical absorption spectra, which allowed us to construct the energy-level schemes and to determine the corresponding set of crystal-field (CF) and exchange-interaction (EI) parameters. The found CF parameters and the parametrized Ho-Fe exchange interaction were further used to simulate the registered spectral changes in the magnetically ordered phases and the magnetic properties of the compound. This revealed a strong noncollinearity of Ho sublattices in the exchange Ho-Fe field due to a nondiagonal component of the Ho^{3+} local magnetic susceptibility. To check the derived magnetic structure, the single-crystal neutron diffraction experiments were performed. As a result, a comprehensive noncontradictory picture of the iron and holmium magnetic order is obtained and physically justified crystal-field and exchange parameters are found, which creates a solid basis for understanding multiferroic properties of the compound [22,23].

The paper is organized as follows. In Sec. II, we describe the samples used and the details of optical and neutron diffraction measurements. Section III reports on the temperature-dependent optical spectra. Section IV is devoted to the theoretical consideration of the CF excitations of holmium ions and the magnetic properties of $HoFe_3(BO_3)_4$. Section V describes the results of the single-crystal neutron diffraction measurements. The paper ends with the Conclusion.

II. EXPERIMENT

$HoFe_3(BO_3)_4$ single crystals were grown by the solution-melt method [24] using the $Bi_2Mo_3O_{12}$-based flux: 75 wt. % $(Bi_2Mo_3O_{12} + 3\,B_2O_3 + 0.5\,Ho_2O_3)$ + 25 wt. % $HoFe_3(BO_3)_4$. The saturation temperature of such a solution melt was found to be $T_{sat} = 960 \pm 3$ °C. Crystals grown on seeds at a rate of no more than 1 mm/day had a size of about $5 \times 7 \times 7\,mm^3$. They had a dark green color and good optical quality. The crystals for optical measurements were oriented using their morphology and optical polarization methods. Samples were cut either perpendicular or parallel to the c axis and polished to the thickness of 0.15 mm.

Transmission spectra of the holmium iron borate were registered in a spectral range 4000–23 000 cm^{-1} with the resolution 0.1 cm^{-1} using a Fourier spectrometer Bruker IFS 125 HR. For the temperature measurements in a range 4–150 K a closed helium-cycle cryostat Cryomech ST403 was used. The temperatures 1.7–4.0 K were achieved using a helium-vapor cryostat with vapor pumping. The temperature was stabilized with an accuracy of ±0.05 K at $T < 70$ K and ±0.1 K at $T > 70$ K. We made use of either unpolarized light propagating along the c axis of the crystal ($\boldsymbol{k} \parallel c$, $\boldsymbol{E}$, $\boldsymbol{H} \perp c$: α polarization) or linearly polarized light incident perpendicular to the c axis ($\boldsymbol{k} \perp c$, $\boldsymbol{E} \perp c$, $\boldsymbol{H} \parallel c$: σ polarization; $\boldsymbol{k} \perp c$, $\boldsymbol{E} \parallel c$, $\boldsymbol{H} \perp c$: π polarization).

The single-crystal neutron diffraction experiments, including the technique of the polarized neutrons, were carried out at the diffractometer 6T2 (LLB-Orphée, CEA, Saclay). To determine the ferromagnetic components, we used the "flipping ratio" method in a vertical magnetic field up to 6.2 T. Neutrons of wavelength 1.4 Å were monochromatized by a vertically focusing graphite crystal and polarized by a supermirror bender. A mm-size single crystal was mounted inside a so-called "Displex" cryostat that provided sample temperatures in the range 1.5–300 K. The crystal was orientated with the a axis upright along the vertical magnetic field ($\boldsymbol{B} \perp c$).

III. OPTICAL SPECTRA OF $HoFe_3(BO_3)_4$: ENERGY LEVELS OF Ho^{3+} IN THE PARAMAGNETIC AND TWO MAGNETIC PHASES

The holmium iron borate has the most complicated optical spectrum among the RE iron borates. We are not aware of any attempts to find the CF parameters for Ho^{3+} ions in $HoFe_3(BO_3)_4$ on the basis of spectroscopic results. The spectra in a broad spectral and temperature range of a sample in the paramagnetic and magnetically ordered states are necessary for that. In Ref. [20], high-resolution α-polarized absorption spectra in the range 4950–8750 cm^{-1} at 6, 30, and 60 K were presented without a detailed analysis. The authors of Ref. [25] published the σ- and π-polarized absorption spectra of a $HoFe_3(BO_3)_4$ single crystal at a resolution of 1.5 cm^{-1} in the range 8500–24 050 cm^{-1} but only at low temperatures (2–30 K); they analyzed the spectra under the assumption of the D_3 point symmetry group at holmium sites, which resulted in wrong conclusions. Here we report on thorough high-resolution (0.1 cm^{-1}), broad-band (4000–23 000 cm^{-1}), polarized temperature-dependent (1.7–150 K) optical absorp-

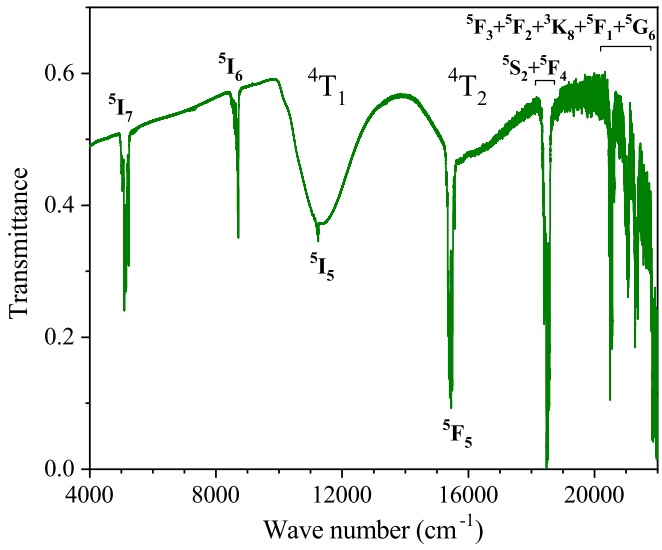

FIG. 1. Broadband transmission spectrum of a $HoFe_3(BO_3)_4$ single crystal at 40 K. The final states of the Ho^{3+} (Fe^{3+}) transitions from the ground multiplet $^5I_8$ ($^6S_{5/2}$) are indicated. $^4T_1$ and $^4T_2$ are the sets of six Kramers doublets of the Fe^{3+} ions, corresponding to orbital quasitriplet states with the total spin $S = 3/2$.

tion measurements of $HoFe_3(BO_3)_4$ single crystals in the paramagnetic and two magnetic phases.

A transmission spectrum of $HoFe_3(BO_3)_4$ in the whole spectral region is shown in Fig. 1. The wide bands designated $^4T_1$ and $^4T_2$ correspond to *d-d* optical transitions between the ground and excited states of the $3d^5$ electronic shell of the Fe^{3+} ions. Those are the absorption bands of iron that determine the green color of iron borate single crystals. Intensive absorption in the region of wave numbers above 24 000 cm^{-1} is connected with the charge-transfer transitions [26]. Numerous narrow spectral lines are due to *f-f* optical transitions between the energy levels of the $4f^{10}$ electronic shell of the Ho^{3+} ions. After subtracting the *d-d* absorption bands (measured in $GdFe_3(BO_3)_4$, where *f-f* transitions start at energies above $\sim$ 30 000 cm^{-1}), one gets the spectra of the *f-f* transitions.

Figure 2 shows thus obtained α-polarized spectra for several optical multiplets of Ho^{3+} in the low-symmetry $P3_121$ phase of $HoFe_3(BO_3)_4$ at different temperatures, both above (150 and 60 K) and below (30 and 5 K) $T_N = 38.5$ K but above the spin-reorientation transition, $T_{SR} = 4.7 \pm 0.2$ K [20]. The spectra are complex and contain many lines. Some of them disappear when the temperature drops [e.g., 5*D*, 5*A*, 6*A*, etc., in Fig. 2(c)]. These lines begin at the excited levels of the ground multiplet $^5I_8$ (numbered 2, 3, etc., in order of increasing their energy above the ground state, designated as 1), the population of which decreases with decreasing temperature. In this paper, notations of spectral lines contain the initial and final levels of optical transitions; CF levels of a given excited multiplet are labeled by capital letters (*A*, *B*, etc.). CF multiplets arising from the levels of a free non-Kramers ion (like Ho^{3+}) placed into the D_3 or C_2 symmetry positions are presented in Table V (Appendix A).

As the ground multiplet of the Ho^{3+} ion is $^5I_8$, there are a lot of CF levels in the ground CF manifold of Ho^{3+} in $HoFe_3(BO_3)_4$ (see Table V in Appendix A), which strongly complicates the line identification. A detailed study of the temperature dependencies of the line positions and intensities, taking into account the selection rules for optical transitions (Table VI in Appendix A), and including the modeling of intensities, based on the Boltzmann distribution for the CF levels' populations, allowed us to identify the spectral lines and to find the energies of 12 excited (out of 16) CF sublevels of the ground $^5I_8$ multiplet and many sublevels of the excited multiplets in the paramagnetic (60 K) and the easy-plane (5 K) and easy-axis (1.7 K) magnetic phases of $HoFe_3(BO_3)_4$ (see Table I; a complete table is given in the Supplemental Material [27]).

The spectrum of paramagnetic $HoFe_3(BO_3)_4$ consists of a set of overlapping lines, a significant part of which corresponds to transitions from numerous excited CF levels of the ground $^5I_8$ multiplet. It is not possible to unambiguously identify the observed spectral lines having only the spectra of the paramagnetic crystal. With magnetic ordering of the crystal, spectral lines noticeably narrow. At the lowest temperature of 1.7 K, only the ground level is populated, and well-resolved lines corresponding to optical transitions from the ground state to the CF levels of excited multiplets are observed (see Fig. 3). Precise positions of these levels are listed in column 9 of Table I (see also Table SI in the Supplemental Material [27]).

Due to a better spectral resolution, we were able to deliver a more detailed picture of the lowest-temperature energy levels than in Ref. [25]. Appreciable differences (up to 7 cm^{-1}) between the frequencies of transitions measured in the present work and Ref. [25] were found for the $^5F_4$ and $^5F_5$ optical multiplets. For the $^5I_7$ and $^5S_2$ manifolds, the number of observed lines coincides with the number predicted for the C_2 symmetry, for $^5I_6$, and $^5I_5$ one line is missing, and for $^5F_5$ and $^5F_4$ two lines were not found.

At the spin-reorientation, which occurs at $T_{SR} = 4.7$ K, most of the levels only shift slightly (0.5–2.0 cm^{-1}) from their positions at 1.7 K, but a part of optical doublets merge into a single level—e.g., instead of two lines, 5155.3 and 5159.3 cm^{-1} at 1.7 K [see Fig. 3(c)], only one line, 5156.3 cm^{-1}, is observed at 5 K [Fig. 3(a)]; lines 8709 and 8715 cm^{-1} at 1.7 K [Fig. 3(d)] merge into line 8711 cm^{-1} at 5 K [Fig. 3(b)]. With further increasing the temperature above T_N, several closely spaced lines at 5 K, which can be assigned to transitions in the magnetically nonequivalent ions in the easy-plane magnetic phase (see Sec. IV below), also merge into a single line.

It is natural to assume that the splitting of the doubly degenerate Γ_3 levels of the D_3 point symmetry group into a pair $\gamma_1 + \gamma_2$ of the C_2 one, that takes place at the $R32 \rightarrow P3_121$ structural phase transition, is small but grows under the influence of an in-plane internal magnetic field, which appears in the easy-plane magnetic state at $T_N > T > T_{SR}$. The positions of thus identified pairs of singlets $\gamma_1 + \gamma_2$ correlate with the energies of Γ_3 doublets in the energy pattern of the impurity Ho^{3+} ions in $YAl_3(BO_3)_4$, which substitute for Y^{3+} at sites with the D_3 symmetry [28] (see Table I and Table S1 in the Supplemental Material [27]).

It is worth noting that the analysis of the low-temperature magnetic properties and the polarized optical spectra of $HoFe_3(BO_3)_4$ performed earlier [25,29–32] in the framework of the D_3 point symmetry group (in which, in particular,

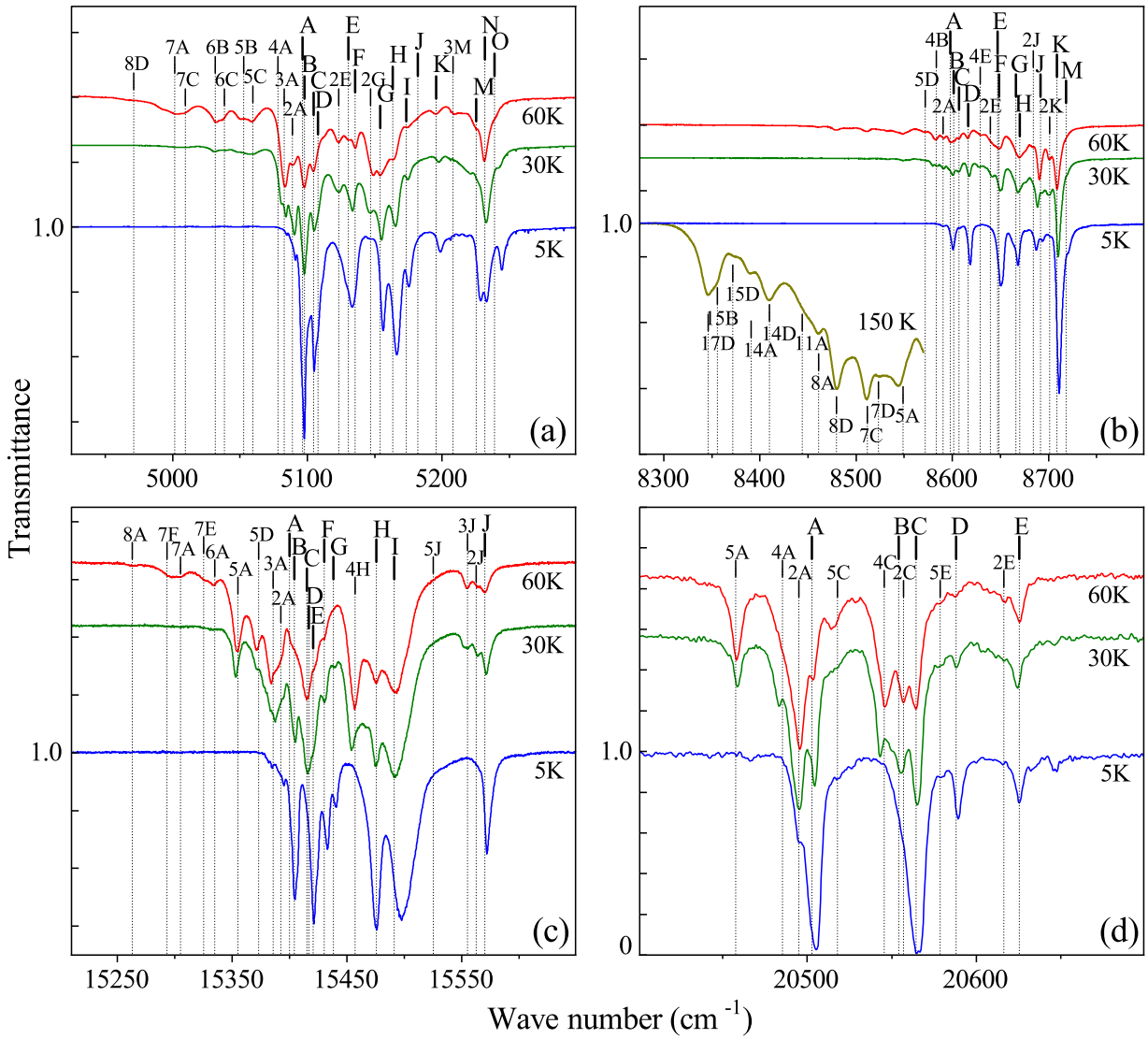

FIG. 2. The α-polarized transmission spectra of a 0.15-mm-thick single crystal of $HoFe_3(BO_3)_4$ [after subtraction of the spectra of $GdFe_3(BO_3)_4$] in the region of optical transitions from the ground $^5I_8$ multiplet to (a) $^5I_7$, (b) $^5I_6$, (c) $^5F_5$, and (d) $^5F_3$ excited multiplets of Ho^{3+} at the temperatures below $T_S = 360$ K: (150 and 60 K) $> T_N$; $T_N >$ (30 and 5 K) $> T_{SR}$. The vertical scale division is 0.2. The spectra at 30 and 60 K are vertically shifted.

Ho^{3+} has a Γ_3 doublet ground state) has no sense since the C_2 -symmetry CF component removes any orbital degeneracy and changes optical selection rules. If the ground state were a Γ_3 doublet, all the spectral lines would split into two components in the magnetically ordered state, which is not the case experimentally. Another point which was not taken into account in Refs. [25,29–31] is that an internal exchange magnetic field at holmium sites in the magnetically ordered state mixes the wave functions that transform in accordance with different irreducible representations (IRs), which leads to the appearance of previously forbidden spectral lines [33]. Taking into account both these circumstances, one can explain polarizations and intensities of the lines in the spectra of $HoFe_3(BO_3)_4$, based on a singlet ground state and invariable local positional symmetry for Ho^{3+} in both the ground and excited states, without an assumption of a strong change of the local symmetry in some excited states in the easy-plane magnetic phase, made in Refs. [25,29–31]. Thus, the present study clarifies the physics of the RE subsystem in this important multiferroic.

The set of holmium CF levels in the paramagnetic and two magnetic phases of $HoFe_3(BO_3)_4$ obtained in this section is further used to perform CF calculations. Physically grounded CF parameters derived below from the analysis of the spectroscopic data form a solid basis for studying magnetic, magnetoelectric, and other properties of the compound.

IV. THEORETICAL ANALYSIS

In this section, we construct an effective Hamiltonian for describing the spectroscopic and magnetic properties of $HoFe_3(BO_3)_4$ and find its parameters, based on calculations within the framework of the exchange-charge model (ECM) [34] and further fitting to experimental data. Next, we use this Hamiltonian to calculate the temperature dependence of the magnetic susceptibility tensor of the Ho subsystem in the

TABLE I. Energies (cm^{-1}) of CF levels of Ho^{3+} in Ho:$YAl_3(BO_3)_4$ [28] and $HoFe_3(BO_3)_4$ in the paramagnetic ($T = 60\,K > T_N = 38.5\,K$) and two magnetic phases, $T_N > 5\,K > T_{SR} = 4.7\,K$ and $T < T_{SR}$. The data for $T < T_{SR}$ are given at 1.7 K. The levels also registered at 2 K in Ref. [25] are marked by an asterisk. Γ_3 is the two-dimensional irreducible representation (IR) of the D_3 point symmetry group, γ_1 and γ_2 are one-dimensional IRs of the C_2 group. Here, the data for the two lowest multiplets are given. For a complete table see Supplemental Material [27].

	Ho: $YAl_3(BO_3)_4$			$HoFe_3(BO_3)_4$					
	CF energies			Shifts $\Delta = E(5\,K) - E(60\,K)$				CF energies	
				Expt.		Theor			
$^{2S+1}L_J$	Expt. [28]	Expt. 60 K	Theor. $T > T_N$	Ho1	Ho2	Ho1	Ho2	Expt $T < 4.7\,K$	Theor $T < 4.7\,K$
1	2	3	4	5	6	7	8	9	10
$^5I_8$ 1	$0\Gamma_3$	0	$0\gamma_1$			0	0	0	0
2		7.5	7.92 γ_2			0.3	3.3	9*	12
3	12.3 Γ_3	14.1	12.7 γ_1			4.7	1.6	12*	13.8
4		18.3	18.4 γ_2			4.4	3.8	21*	23.0
5	14.3	45	48.1 γ_1			2.3	1.4	47*	49.7
6	35	66	64.3 γ_2			2.4	4.2	67*	67.4
7	126	95	93.5 γ_1			2.2	2.3		96.2
8	136 Γ_3	137	134.7 γ_1			2.6	2.0		134
9			140.6 γ_2			1.1	2.1		140
10	148 Γ_3		146.5 γ_2			3.7	2.7		150
11		154	151.2 γ_1			2.6	3.4		157
12	175	175	173.6 γ_2			1.7	1.7		177
13	211 Γ_3		202.4 γ_2			3.0	2.2		204
14		207	210.8 γ_1			2.0	2.8		214
15	262 Γ_3	246	251.7 γ_1			1.2	2.0		254
16			254.9 γ_2			2.7	1.2		258
17	283	272	272.6 γ_1			4.1	5.4		275
^5I_7A	5 099.2 Γ_3	5096.5	5095.4 γ_2	1.2	0	1.1	0.5	5095.9	5094.0
B		5097.7	5097 γ_1		3.3	1.3	3.6	5098	5101.8
C	5101	5104.5	5104.1 γ_2	3.0	0.5	3.6	1.7	5102	5103.2
D	5104	5108	5106.5 γ_1		3.0	3.5	3.7	5114	5110.9
E	5110 Γ_3	5130.6	5131.1 γ_2	2.5		2.3	−1.1	5128.2	5129.3
F		5135.5	5131.6 γ_1			2.4	6.0	5138.8	5136.8
G		5154	5158.2 γ_2		2.2	2.3	2.4	5155.5	5159.6
H	5168	5163.2	5177 γ_1		2.8	2.0	2.2	5165.8	5177.7
I	− Γ_3	5173.5	5181.2 γ_2		2.0	2.6	2.5	5177.9	5180.7
J	5191	5181.9	5184.1 γ_1			2.6	2.4	5196.9	5193
K	5217.5 Γ_3	5195.6	5203.7 γ_2		3.1	2.2	2.5		5204.6
L			5205 γ_1			2.5	2.4		5207.7
M	5249 Γ_3	5225.4	5232.5 γ_2		3.2	1.6	2.4	5226.4	5234.0
N		5231.6	5235.1 γ_1		1.4	2.6	1.4	5235	5237.1
O	5262	5239	5245.8 γ_2		5.3	3.4	4.4	5243.5	5247.5

paramagnetic and antiferromagnetic phases of $HoFe_3(BO_3)_4$. Comparing the results of these calculations with the experimental data, we find that the Ho subsystem gives a dominant contribution to the magnetic susceptibilities of $HoFe_3(BO_3)_4$, despite a substantial suppression of this contribution by the Fe-Ho staggered exchange fields that induce antiferromagnetic order in the Ho subsystem below T_N.

We follow the approach used by us earlier in Refs. [35–38] and start from a consideration of independent Ho^{3+} ions in the effective local magnetic fields $\boldsymbol{B}_{loc}$. To account for the exchange fields, the anisotropic Fe-Ho exchange interaction in the mean-field approximation is introduced. We consider magnetic properties of the iron subsystem following our previous study of the isostructural yttrium iron borate [39] (it should be noted that holmium and yttrium iron borates have almost the same Néel temperatures, $T_N = 38.5$ and 38 K, respectively). In the framework of this approach, we calculate the energy spectra of Ho^{3+} ions in the antiferromagnetic easy-plane and easy-axis phases. We also calculate the temperature dependencies of the magnetic susceptibilities and magnetic moments of Ho^{3+} ions induced by the spontaneously ordered magnetic moments of iron ions in $HoFe_3(BO_3)_4$ and compare them with the measured ones.

A. Effective Hamiltonian and magnetic susceptibilities of a Ho^{3+} ion in the crystal field

The primitive cell of $HoFe_3(BO_3)_4$ with the $P3_121$ structure contains three formula units. FeO_6 octahedra share

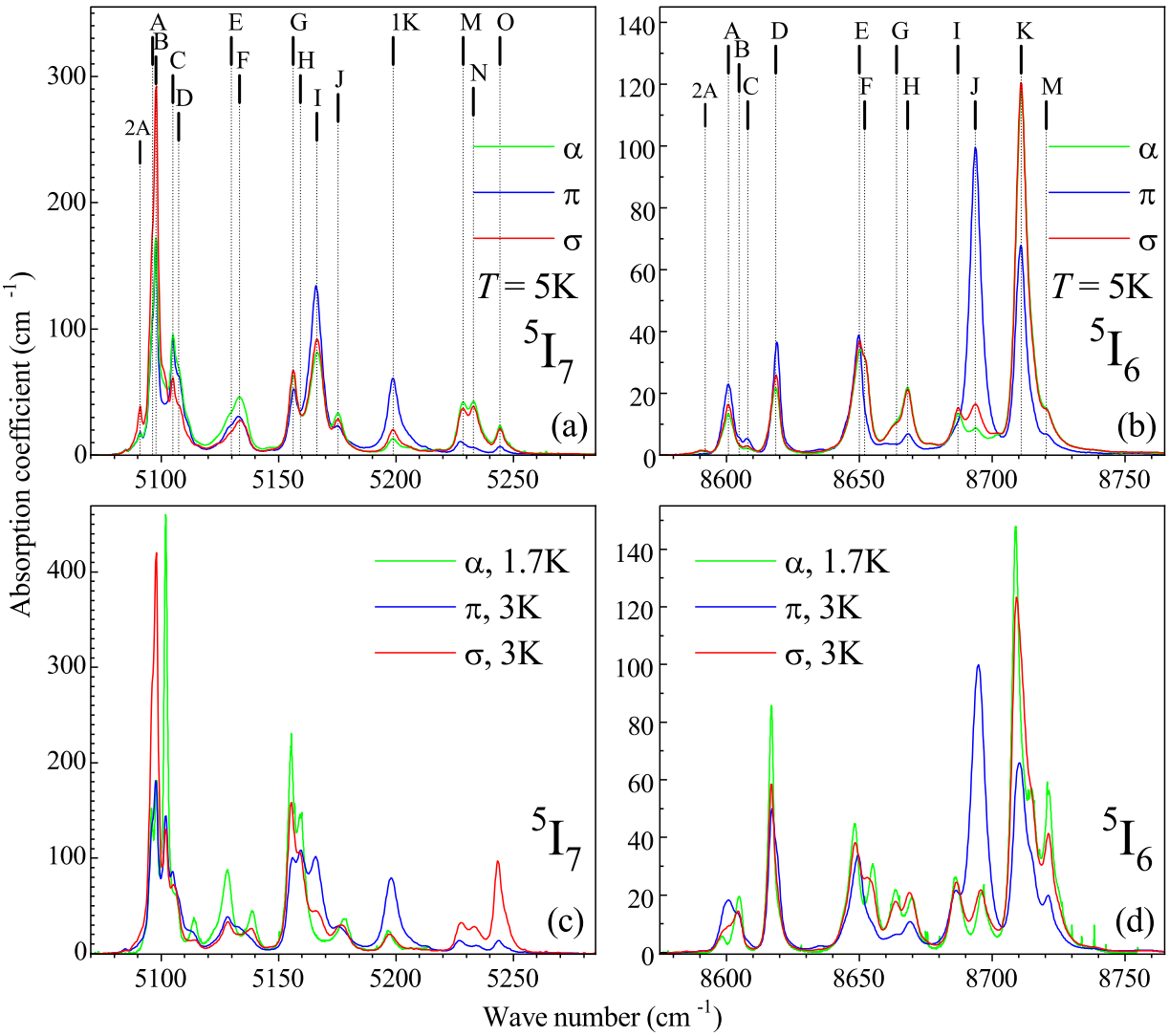

FIG. 3. The α-, π-, and σ-polarized absorption spectra of a $HoFe_3(BO_3)_4$ single crystal at (a),(b) $T_N > 5\,K > T_{SR}$ and (c),(d) 1.7 K, $3\,K < T_{SR}$ in the spectral regions of the (a),(c) $^5I_7$ and (b),(d) $^5I_6$ multiplets.

common edges forming isolated helical chains along the trigonal c axis. The chains are interconnected by BO_3 triangles and isolated HoO_6 distorted prisms. There are three crystallographically equivalent but magnetically nonequivalent Ho^{3+} ions shifted by $c/3$ along the c axis relative to each other and connected by the $2\pi/3$ rotations around the c axis. They occupy the Wyckoff positions $3a$ with the local symmetry C_2 and coordinates $(x, 0, 1/3)$, $(0, x, 2/3)$, and $(-x, -x, 0)$. Fe atoms occupy two different crystallographic sites. Fe1 are in the $3a$ positions, the same as Ho. Fe2 reside in the $6c$ positions with the local symmetry C_1 and coordinates (x, y, z), $(-y, x-y, z+1/3)$, $(-x+y, -x, z+2/3)$, $(y, x, -z)$, $(x-y, -y, -z+2/3)$, $(-x, -x+y, -z+1/3)$. There are two types of nonequivalent helicoidal chains of the FeO_6 octahedra containing the Fe1 or Fe2 ions.

Spectral and magnetic properties of an isolated Ho^{3+} ion with the ground electronic configuration $4f^{10}$ in a dielectric crystal can be described using the Hamiltonian

$$H_0 = H_{FI} + H_{CF} + H_Z, \tag{1}$$

where

$$H_{FI} = \zeta \sum_j \boldsymbol{l}_j \boldsymbol{s}_j + \alpha \hat{\boldsymbol{L}}^2 + \beta \hat{G}(G_2) + \gamma \hat{G}(R_7) + \sum_q (F^q \hat{f}_q + P^q \hat{p}_q + T^q \hat{t}_q + M^q \hat{m}_q) \tag{2}$$

is the free-ion Hamiltonian written in a standard form [40] (see details in the Supplemental Material [27]). The Hamiltonian H_{CF} stands for the energy of localized $4f$ electrons (labeled by the index j) in a static crystal field, and $H_Z = -\boldsymbol{m}\boldsymbol{B}_{loc}$ is the Zeeman energy. Here,

$$\boldsymbol{m} = -\mu_B \sum_j (k\boldsymbol{l}_j + 2\boldsymbol{s}_j) \tag{3}$$

is the magnetic moment operator of a holmium ion, μ_B is the Bohr magneton, k is the orbital reduction factor, and $\boldsymbol{l}_j$ and $\boldsymbol{s}_j$ are orbital and spin moments of electrons.

The CF Hamiltonian in the local right-handed Cartesian system of coordinates with the origin at the selected Ho^{3+} ion and with the z axis along the crystallographic c axis and the x

axis along the C_2 symmetry axis is determined by 15 real CF parameters B_q^p:

$$H_{\mathrm{CF}} = \sum_{j=1}^{10} \{B_0^2 C_0^{(2)}(j) + B_0^4 C_0^{(4)}(j) + B_0^6 C_0^{(6)}(j) + iB_{-3}^4 [C_{-3}^{(4)}(j) + C_3^{(4)}(j)] + iB_{-3}^6 [C_{-3}^{(6)}(j) + C_3^{(6)}(j)] + B_6^6 [C_{-6}^{(6)}(j) + C_6^{(6)}(j)] + iB_{-1}^2 [C_{-1}^{(2)}(j) + C_1^{(2)}(j)] + B_2^2 [C_{-2}^{(2)}(j) + C_2^{(2)}(j)] + iB_{-1}^4 [C_{-1}^{(4)}(j) + C_1^{(4)}(j)] + B_2^4 [C_{-2}^{(4)}(j) + C_2^{(4)}(j)] + iB_{-1}^6 [C_{-1}^{(6)}(j) + C_1^{(6)}(j)] + B_2^6 [C_{-2}^{(6)}(j) + C_2^{(6)}(j)] + B_4^4 [C_{-4}^{(4)}(j) + C_4^{(4)}(j)] + B_4^6 [C_{-4}^{(6)}(j) + C_4^{(6)}(j)] + iB_{-5}^6 [C_{-5}^{(6)}(j) + C_5^{(6)}(j)]\}, \quad (4)$$

where $C_q^{(p)}$ is the spherical tensor operator of the rank p. Six parameters, namely, B_0^2, B_0^4, B_{-3}^4, B_0^6, B_{-3}^6, and B_6^6, in the first two lines of Eq. (4) define the dominant CF component of the trigonal symmetry and the other nine parameters refer to the CF component of the C_2 symmetry. The initial values of the CF parameters were calculated in the framework of ECM [34] using the structural data from Refs. [18,41] (see details in the Supplemental Material [27]). The results of the calculation are presented in Table II (columns 5 and 6, respectively).

The obtained CF parameters correlate well with the results of similar calculations for the Tb^{3+} and Dy^{3+} ions in terbium and dysprosium iron borates [37,42]. It should be noted that the calculated parameters of the trigonal CF component for both sets of structural parameters from Refs. [18,41] are almost the same, but the parameters of the low-symmetry (C_2) CF component in columns 5 and 6 differ markedly. These parameters are highly sensitive to the crystal structure.

Next, the initial CF parameters were varied to fit the measured energies of the transitions between the CF levels of the Ho^{3+} ions and the temperature dependencies of the static magnetic susceptibilities of $HoFe_3(BO_3)_4$ in the paramagnetic phase. In particular, the variational procedure involved the numerical diagonalization of the Hamiltonian (1) operating in the total space of 1001 states of the electronic $4f^{10}$ configuration and calculations of the matrices of the Ho^{3+} moment components in the basis of the corresponding eigenfunctions. The final set of the CF parameters is presented in column 7 of Table II. The relatively large differences between the final and initial values of the second-rank CF parameters, which are most sensitive to the long-range Coulomb interactions, are probably caused by neglecting the redistribution of electron density in BO_3 triangles with strong covalent bonds.

TABLE II. Crystal-field parameters B_q^p (cm^{-1}) for RE iron borates $REFe_3(BO_3)_4$ with the $P3_121$ structure. In the $P3_221$ structure, the parameters with $q = -1$, -3, and -5 have opposite signs.

		RE = Eu	Tb	Dy	Ho			Er
p	q	[43]	[37]	[42]	(this work)			[38]
1		2	3	4	5[a]	6[a]	7	8
2	0	484	434	404	182	186	370	366
4	0	−1255	−1256	−1192	−1161	−1165	−1123	−1103
4	−3	619	608	554.4	494	492	509.4	485.4
6	0	404	352	328	310	315	326	309
6	−3	80	73	70.3	62	61	63.3	58.3
6	6	290	270	232	190	190	235	222
2	−1	39	38	58.4	158	69	89.4	89.4
4	−1	−76	−66	−49.2	−55	−45	−54.2	−54.2
6	−1	−32	−27	−7.4	−20	0.1	−16.4	−16.4
2	2	54	54	69.4	95	121	67.4	67.4
4	2	102	82	101.2	98	106	85.2	60.2
6	2	−11	−8	−14	−4	−12	−8	−13
4	4	−26	−23	15.9	−13	15	13.1	10.1
6	4	−31	−27	31.4	6	33	2.6	3.6
6	−5	−131	−91	−79	−106	−100	−75	−70

[a]CF parameters calculated in the frame of ECM by making use of the lattice structure data from Refs. [18] (column 5) and [41] (column 6).

The computed CF energies and symmetry properties (IRs of the C_2 point symmetry group) of corresponding wave functions of the Ho^{3+} ions (column 4 in Table I) match satisfactorily the experimental results (column 3 in Table I above and in the Supplemental Material [27]). It should be noted that the CF parameters used in Ref. [32] to explain the magnetic properties of $HoFe_3(BO_3)_4$ lead to a substantially incorrect picture of the energy spectrum.

We note that the values of the six CF parameters B_0^2, B_0^4, B_{-3}^4, B_0^6, B_{-3}^6, and B_6^6, which determine the trigonal CF component, change monotonically along the series of RE iron borates (see Table II). The remaining nine CF parameters that refer to the CF component of the C_2 symmetry are found with lower accuracy, because of their relatively small influence on the multiplet splittings. However, just these CF parameters determine some specific properties of RE iron borates in the $P3_121$ phase, in particular, a magnetic anisotropy of the Ho^{3+} ions in the ab plane and a presence of the off-diagonal terms in their magnetic susceptibility tensor.

Figure 4 (dashed lines) shows the calculated temperature dependencies of the magnetic susceptibility tensor components $\chi_{\mathrm{Ho},\alpha\beta} = M_{\mathrm{Ho},\alpha}(B_\beta, T)/B_\beta$ of the Ho^{3+} ion (here, $\boldsymbol{M}_{\mathrm{Ho}}$ is the magnetic moment induced by the external magnetic field $\boldsymbol{B}$). In these calculations, we used the Hamiltonian (1) and the orbital reduction factor $k = 0.92$, which was estimated by a comparison of the calculated and measured high-temperature susceptibilities of $HoFe_3(BO_3)_4$.

All CF energy levels are orbital singlets, and the temperature dependencies of single-holmium-ion susceptibilities reach a plateau at low temperatures. The important features of the holmium susceptibilities are a noticeable magnetic anisotropy at $T < 20$ K ($\chi_{\mathrm{Ho},\parallel} > \chi_{\mathrm{Ho},\perp}$) and a large value of the off-diagonal component $\chi_{\mathrm{Ho},yz}$ of the susceptibility tensor at $T < T_{\mathrm{N}}$.

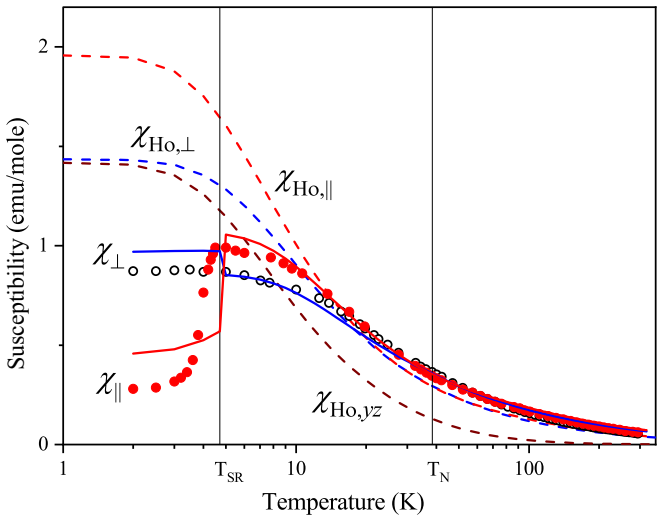

FIG. 4. Calculated (dashed lines) temperature dependencies of the longitudinal $\chi_{\mathrm{Ho},\parallel} = \chi_{\mathrm{Ho},zz}$, transversal $\chi_{\mathrm{Ho},\perp} = (\chi_{\mathrm{Ho},xx} + \chi_{\mathrm{Ho},yy})/2$ (the average value over three magnetically inequivalent Ho^{3+} ions in the unit cell for the field in the *ab* plane), and the off-diagonal $\chi_{\mathrm{Ho},yz}$ magnetic susceptibilities of a Ho^{3+} ion in the local Cartesian coordinates with the *x* axis along the C_2 axis in the *ab* plane and the *z* axis along the *c* axis. The relation for $\chi_{\mathrm{Ho},\perp}$ is valid not only in the paramagnetic phase but also in the easy-plane phase, due to the domains with the Fe spins aligned along the three C_2 symmetry axes. Also shown are simulated (solid lines) and measured [18] longitudinal ($\chi_{\parallel}$, closed circles) and transversal ($\chi_{\perp}$, open circles) susceptibilities of $HoFe_3(BO_3)_4$, $B = 0.1$ T.

To unveil the physical origin of the observed low-temperature magnetic anisotropy, we carry out a simplified analytical consideration of the Van Vleck susceptibility $\chi_{\mathrm{Ho},\alpha\gamma}$ in the truncated basis of four lower singlets of the ground multiplet, using the following expression:

$$\chi_{\mathrm{Ho},\alpha\gamma} = N_A \sum_{p=1}^{4}\sum_{q=1}^{4} \frac{(m_{\alpha,pq}m_{\gamma,qp} + m_{\gamma,pq}m_{\alpha,qp})\exp(-\beta E_p)}{Z(E_q - E_p)}. \tag{5}$$

Here N_A is the Avogadro number, $\beta = 1/k_BT$, k_B is the Boltzmann constant, E_p are energies of the CF levels (see column 4 in Table I), and $Z = \sum_{p=1}^{4}\exp(-\beta E_p)$ is the partition function. The calculated nonzero matrix elements of the magnetic moment components in the space of four lower sublevels are the following (in units of μ_B): $m_{x,13} = -6.6i$, $m_{x,24} = -5.51i$, $m_{y,12} = -3.97$, $m_{y,14} = 0.89$, $m_{y,23} = 0.43$, $m_{y,34} = -3.0$, $m_{z,12} = -5.46$, $m_{z,14} = 0.41$, $m_{z,23} = 1.05$, $m_{z,34} = -4.56$. The operators of the magnetic moment components m_y and m_z connect the ground state γ_1 with the first excited sublevel γ_2, but the m_x operator can mix the ground state only with the higher-lying states γ_1. In particular, for $T = 5$ K, we get (in units of emu/mole) $\chi_{\mathrm{Ho},zz} = \chi_{\mathrm{Ho},xx} = 1.6$, $\chi_{\mathrm{Ho},yy} = 0.87$, $\chi_{\mathrm{Ho},yz} \approx \chi_{\mathrm{Ho},\perp} = 1.2$; these values agree satisfactorily with the results of computations presented in Fig. 4. Thus, one can conclude that main contributions to the magnetic susceptibility of the holmium subsystem are made by the 1 $\rightarrow$ 2, 1 $\rightarrow$ 3, and 2 $\rightarrow$ 4 CF virtual transitions (although the latter is frozen at low temperatures, $k_BT \ll E_2$).

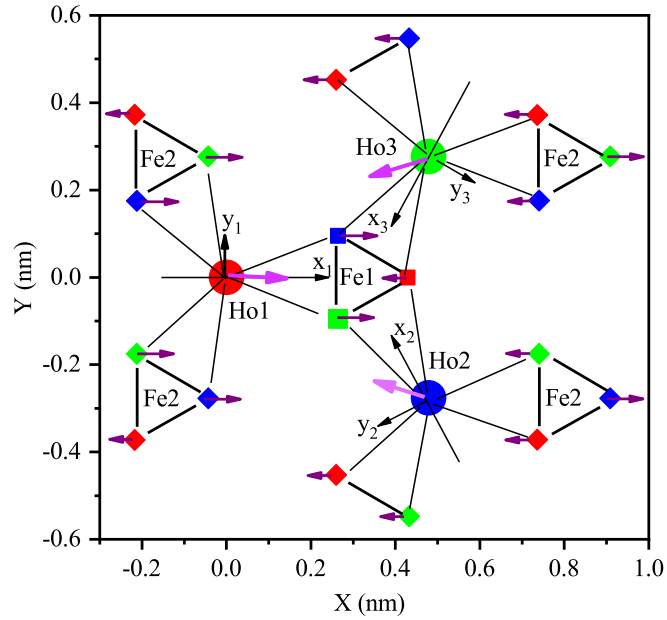

FIG. 5. Projections of the iron and holmium ions and their magnetic moments in the easy-plane phase onto the *ab* crystallographic plane. Color arrows show magnetic moments of iron and holmium ions. The orthogonal x_i and y_i axes ($x_1 \parallel a$, $y_1 \parallel b^*$) are coordinate axes of the local Cartesian frames of Ho ions. Filled (red) symbols correspond to ions belonging to the fixed *ab* plane ($z = 0$), blue and green symbols correspond to ions lying within the planes displaced by $+c/3$ and $-c/3$, respectively, relative to the basal plane $z = 0$.

Comparison with the experimental data [18] (see Fig. 4) and with the susceptibilities of the iron subsystem [39] evidences a dominant contribution of the holmium subsystem into the magnetic susceptibilities of $HoFe_3(BO_3)_4$ in the paramagnetic phase and a partial suppression of this contribution due to the magnetic order induced in the Ho subsystem by the exchange Ho-Fe interactions below the Néel temperature.

B. Exchange interactions between Fe^{3+} and Ho^{3+} ions and the magnetic structures in $HoFe_3(BO_3)_4$

In search of a mechanism that could suppress an excessively strong calculated longitudinal susceptibility of the holmium ions in magnetically ordered phases, we introduce the bilinear anisotropic exchange interactions between the nearest-neighbor Fe^{3+} and Ho^{3+} ions with the total spin moments $\boldsymbol{S}_{\mathrm{Fe}}$ and $\boldsymbol{S}_{\mathrm{Ho}}$, respectively:

$$H_{\mathrm{exch}} = -2\sum_{\alpha=x,y,z} J_{fd,\alpha}S_{\mathrm{Fe},\alpha}S_{\mathrm{Ho},\alpha}. \tag{6}$$

The same as in the previous section, local Cartesian coordinate frames at the corresponding holmium sites are used. In this case, the x_i axes ($i = 1, 2, 3$) projected onto a fixed *ab* plane, cross at the center of the triangle formed by the Fe1 ions, as shown in Fig. 5. It should be noted that the anisotropic *f-d* exchange interactions were introduced also in the previous investigations of iron borates with the *R*32 structure, namely, in the studies of spectral properties of $PrFe_3(BO_3)_4$ [36] and of spin-wave dynamics in $NdFe_3(BO_3)_4$ [44]. Similar to our study of magnetic properties of the iron subsystem in the

yttrium iron borate without a rare-earth magnetic subsystem [39], we neglect possible differences between properties of the Fe1 and Fe2 helical chains. Below, we consider the exchange interaction (6) in the mean-field approximation. The obtained expressions for the exchange fields at holmium ions in the easy-plane and easy-axis phases (where all holmium ions are magnetically equivalent) are given in Appendix B.

The long-range magnetic ordering in iron borates is governed by strong intra- and interchain exchange interactions of iron ions. Recently, a comprehensive study of magnetic properties of the quasi-one-dimensional iron system in $YFe_3(BO_3)_4$, the compound isostructural to $HoFe_3(BO_3)_4$ and with rather close Néel temperature, was carried out in Ref. [39] in the framework of the self-consistent four-particle cluster model. The observed magnetic anisotropy of the easy-plane type with the iron magnetic moments lying in the basal plane, perpendicular to the c axis, was confirmed by simulations. The sixfold magnetic anisotropy in the ab plane has not been studied on the microscopic level (most likely, it originates from the magnetoelastic interactions), however the temperature behavior of the magnetic susceptibilities, the phase transition temperature ($T_N = 38$ K), and the temperature dependence of the spontaneous magnetic moments of iron ions were successfully reproduced by the model based on the assumption of the collinear magnetic structure with the iron moments along the C_2 symmetry axis in the ab planes and antiferromagnetically coupled along the c axis.

There is no competition in $HoFe_3(BO_3)_4$ between the magnetic anisotropies of the iron and holmium subsystems at temperatures higher and close to T_N (at these temperatures, the magnetic susceptibility of the holmium subsystem is approximately isotropic; see Fig. 4). So, we assume the same as in $YFe_3(BO_3)_4$ alignment of the iron magnetic moments in the easy-plane phase of $HoFe_3(BO_3)_4$, namely, along the a axis that coincides with the C_2 symmetry axis of the holmium centers Ho1 lying in the ab planes at $z = \pm nc$, where n is an integer number or zero. In this case, the holmium subsystem contains two magnetically nonequivalent sets of the Ho^{3+} ions, namely, (i) the Ho1 ions and (ii) the Ho2 and Ho3 ions lying in the planes $z = \pm nc + c/3$ and $z = \pm nc - c/3$, respectively. The alignment of the iron moments along the a axis in $HoFe_3(BO_3)_4$ is indirectly confirmed by the results of polarized neutron scattering measurements on $NdFe_3(BO_3)_4$, where the alignment of the iron moments along the a axis was established [45], and by the observation of two different Eu^{3+} optical centers in the easy-plane magnetic phase of $EuFe_3(BO_3)_4$ with the $P3_121$ structure [43]. However, the latter fact does not exclude the alignment along the b^* axis. The further calculations are done assuming the alignment of the iron magnetic moments in the easy-plane phase of $HoFe_3(BO_3)_4$ along the a axis. Nevertheless, the alignment along the b^* axis was also considered. In this case, the results of calculations were in worse agreement with the experimental data.

With decreasing temperature ($20\ \mathrm{K} > T \to 0$), the parallel susceptibility of Ho^{3+} ions increases noticeably faster than the transverse one (see Fig. 4). The resulting uniaxial anisotropy of the holmium subsystem causes the spin-reorientation transition at 4.7 K into an easy-axis magnetic structure with the iron magnetic moments parallel to the c axis.

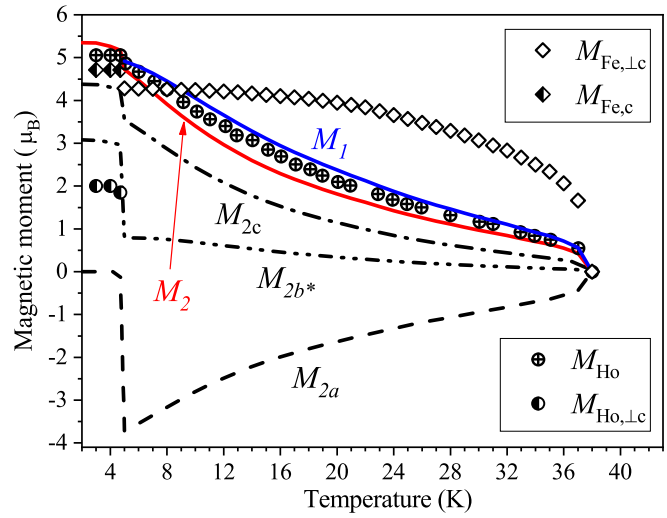

FIG. 6. The calculated temperature dependencies of holmium magnetic moments in the Cartesian coordinate frame of Ho1 ions (see Fig. 5) in the antiferromagnetic phases of $HoFe_3(BO_3)_4$. M_1 and M_2 designate the total values of the Ho1 and Ho2 (Ho3) moments, respectively, M_{2a}, M_{2b*}, and M_{2c} are projections of $\boldsymbol{M}_2$ onto the crystallographic a, b^*, and c axes, respectively. For Ho3, $M_{3a} = M_{2a}$ $M_{3b*} = -M_{2b*}$, $M_{3c} = -M_{2c}$. The data from powder neutron diffraction [18] are shown by symbols.

Further, we calculated the quantum-statistical average values of the holmium magnetic moments $\boldsymbol{M}(\mathrm{Ho}\,k)$, $k = 1, 2, 3$, induced by the spontaneous magnetic moments of iron ions taken from Ref. [39], using the expression

$$M_\alpha(\mathrm{Ho}k, T) = \mathrm{Tr}\{m_\alpha \exp[-\beta H_{\mathrm{eff}}(\mathrm{Ho}k)]\} \times / \mathrm{Tr}\{\exp[-\beta H_{\mathrm{eff}}(\mathrm{Ho}k)]\}, \quad (7)$$

where the effective single-ion Hamiltonian H_{eff} (Ho k) for the Ho1 and Ho2 (Ho3) ions in different phases is defined by Eqs. (B1)–(B3) and (B5) in Appendix B. From a comparison of the calculated holmium moments and susceptibilities of $HoFe_3(BO_3)_4$ in the easy-plane phase with the data of measurements [18], we obtained the following Ho-Fe exchange parameters: $J_{\mathrm{fd},x} = J_{\mathrm{fd},z} = 0.25$ K and $J_{\mathrm{fd},y} = 0.325$ K. The results of calculations are shown in Fig. 4. The effective exchange field for the ground multiplet (with the Landé factor $g_J = 5/4$) $B_{\mathrm{fd},x} = B_{\mathrm{fd},z} = 12 J_{\mathrm{fd},x} S_{\mathrm{Fe}}(g_J - 1)/(g_J \mu_B) \approx 2.2$ T is in a reasonable agreement with the value $B_{\mathrm{ex}} \approx 2$ T found in Ref. [46].

The magnetic moments on the Ho1 sites, induced by the exchange field from the Fe sublattice, and moments of Fe ions lying in the same ab plane have opposite directions. Since the local C_2 symmetry axes of the Ho2 and Ho3 ions deviate from the a axis by the angles $\pm 120^\circ$ (see Fig. 5), symmetry allows the deviation of their moments from the local x axes, i.e., these moments, in contrast to the Ho1 moment, can have both y and z components. For symmetry reasons, these components for Ho2 and Ho3 differ only in sign.

The calculated temperature dependencies of holmium magnetic moments are displayed in Fig. 6. Figure 6 shows that the calculated projections of the Ho2(Ho3) moments onto the ab plane deviate substantially (by the angles φ_k) from the a

axis and that there are rather large components M_{kc} of the Ho2 (Ho3) moment along the c axis in the easy-plane phase. In particular, at $T = 7$ K $\varphi_k = \arctan(M_{kb*}/M_{ka}) = \pm 167^\circ$ ($k = 2, 3$) and the angle $\theta = \arccos(M_{kc}/M_2)$ between the Ho2 (Ho3) moment and the c axis equals 48 ° (132 °). This contradicts the model of the easy-plane magnetic structure with collinear magnetic moments in the *ab* plane of all holmium ions, suggested in Ref. [18] for the interpretation of powder neutron diffraction data. However, it should be noted that the calculated temperature dependencies of the absolute values of the holmium magnetic moments M_1 and $M_2 = M_3$, induced by the spontaneous moments of iron, are in satisfactory agreement with the results of measurements given in [18].

In the easy-axis phase, due to nonzero off-diagonal components of the holmium susceptibility tensors $\chi_{\mathrm{Ho},yz}$, the exchange field created by the z components of the iron moments induces the holmium moment components in the *ab* planes, which order in the 120 ° magnetic structure [18]. The inverse effect would induce the components of Ho2 and Ho3 magnetic moments along the c axis, proportional to the projections of the iron moments on the local y axes of Ho2 and Ho3 ions in the antiferromagnetic easy-plane phase.

Next, we considered the total susceptibility of $HoFe_3(BO_3)_4$ as a sum of susceptibilities of the iron and holmium subsystems. The effective single-ion susceptibilities of iron ions $\chi_{\mathrm{Fe},||}$ and $\chi_{\mathrm{Fe},\perp}$ in the isostructural compound $YFe_3(BO_3)_4$ were presented in Ref. [39]. In the magnetically ordered phases, the holmium susceptibilities $\chi_{\mathrm{Hok},\alpha\beta}$, which determine magnetic moments induced by the external magnetic field $\boldsymbol{B}$, were calculated in the local Cartesian systems of coordinates [according to formulas (B4) and (B5) of Appendix B]. Further, to compare with the observed susceptibilities $\chi_{||}$ and $\chi_\perp$, we averaged the site-specific susceptibilities over three Ho^{3+} ions at the 3*a* sites and took into account the formation of domains. The final expressions for the susceptibilities (per mole) in the easy-plane phase read

$$\chi_{||} = N_A[(\chi_{\mathrm{Ho1},zz} + 2\chi_{\mathrm{Ho2},zz})/3 + 3\chi_{\mathrm{Fe},||}], \tag{8}$$

$$\chi_\perp = N_A[(\chi_{\mathrm{Ho1},xx} + \chi_{\mathrm{Ho1},yy} + 2\chi_{\mathrm{Ho2},xx} + 2\chi_{\mathrm{Ho2},yy})/6 + 3\chi_{\mathrm{Fe},\perp}]. \tag{9}$$

In the easy-axis phase, one should replace $\chi_{\mathrm{Fe},\perp}$ with $\chi_{\mathrm{Fe},||}$ in Eq. (9) and $\chi_{\mathrm{Fe},||}$ with $(2\,\chi_{\mathrm{Fe},\perp} - \chi_{\mathrm{Fe},||})$ in Eq. (8). Note that we neglect here the renormalization of the magnetic moments induced by the external magnetic field, due to the ferromagnetic *f-d* exchange interaction, which slightly increases the computed susceptibilities [38]. The results of calculations are shown in Fig. 4 (solid lines). Probably, the overestimated values of the magnetic susceptibilities in the easy-axis state (Fig. 4) and of the holmium moment projections on the *ab* plane (Fig. 6) are caused by neglecting changes of the CF parameters at the holmium sites at temperatures 2–60 K, where noticeable shifts of the oxygen sublattices were detected in neutron diffraction studies [18].

It is important to note that in the paramagnetic phase, an external magnetic field parallel to the c axis not only polarizes iron moments along the applied field but also induces a chiral transverse magnetic structure in helicoidal iron chains, which is determined by the holmium off-diagonal susceptibility $\chi_{\mathrm{Ho},yz}$ and *f-d* exchange interactions.

Based on the derived magnetic structure, we have also performed the simulations of energy spectra of Ho^{3+} in the magnetic phases of $HoFe_3(BO_3)_4$. They are presented in the Supplemental Material [27]; the calculated energy values show a satisfactory agreement with the experimental data.

In summary, the results of the modeling contradict the magnetic structure suggested earlier on the basis of powder neutron diffraction measurements [18]. Therefore, we performed single-crystal neutron diffraction experiments.

V. SINGLE-CRYSTAL NEUTRON DIFFRACTION

The diffraction patterns were analyzed using the JANA2006 package [47]. Because the single crystal was small, the refinement was not sensitive to extinction and this correction was not included. The atomic coordinates from Ref. [18] were used. The scale factor was refined from the nuclear reflections and was fixed in the refinement of the magnetic reflections. At every temperature point, we measured a set of antiferromagnetic reflections with half-integer indexes $l/2$ and a set of nuclear reflections with integer l indexes.

The analysis of possible magnetic IRs was performed using the program K-SUBGROUPSMAG [48] in the frame of the space group of the paramagnetic phase $P3_121$ (no. 152) and the propagation vector $\boldsymbol{k} = [0,\ 0,\ 1/2]$ reported for the magnetic structure of $HoFe_3(BO_3)_4$ [18]. There are three magnetic IRs of the little group of $\boldsymbol{k}$, namely, *mA*1(1), *mA*2(1), and *mA*3(2) (in the parentheses, the dimension of the IR is given).

A. Low-temperature easy-axis magnetic structure

The refinement of the antiferromagnetic reflections at a temperature of 1.6 K in zero magnetic field unambiguously indicates the *easy-axis* magnetic structure, which can be described only by the one-dimensional IR *mA*2(1) [Shubnikov group $P_c3_22_1$ (no. 154.44)]. This model demonstrates a good agreement with the experiment, a goodness-of-fit parameter for 90 nonequivalent reflections is 2.28. In this space group, the in-plane components of the Ho and Fe1 moments are fixed by the symmetry (see Fig. 7 and Table III), while the Fe2 moment components are symmetry free. The refinement displays a huge error of the azimuthal (in-plane) angle of the Fe2 moment, ∼30 °; therefore, this angle was fixed in refinement.

The observed magnetic structure practically coincides with the *easy-axis* magnetic structure derived from neutron powder diffraction [18]. Small deviations of the Fe spins from the c axis, which, in principle, are expected, bearing in mind the anisotropy of the local Ho^{3+} magnetic susceptibility, are in the limits of several experimental errors.

B. Easy-plane magnetic structure

The *easy-plane* magnetic structure is more complicated. The analysis shows that this state cannot be described by one-dimensional IRs *mA*2(1) or *mA*1(1). Due to a small number of diffraction reflections (∼200) and a large number of refined parameters, the refinement gives many "false" solutions that are practically impossible to resolve. Therefore, we used

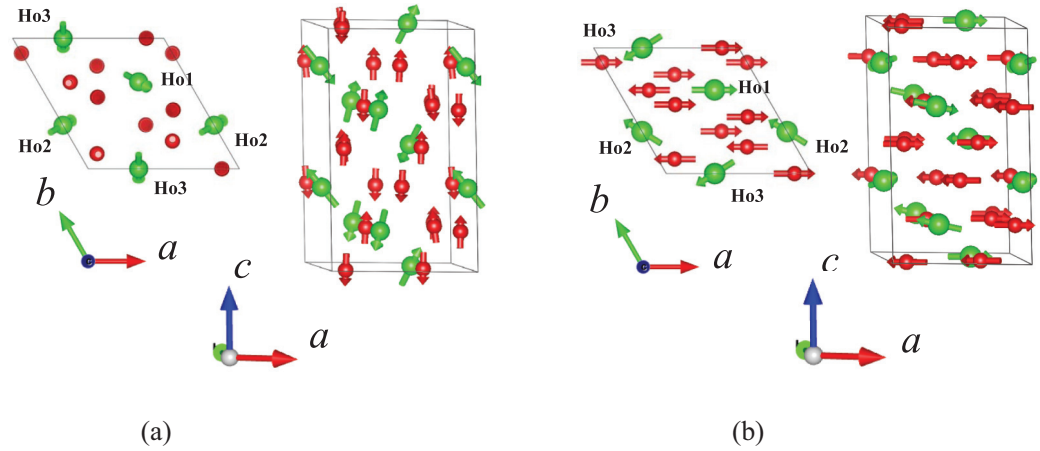

(a) (b)

FIG. 7. (a) *Easy-axis* and (b) *easy-plane* type of the magnetic structure in $HoFe_3(BO_3)_4$ at the temperature of (a) 1.6 K and (b) 7 K. Ho and Fe atoms and moments are shown in green and red color, respectively. A magnetic unit cell, which is twice the chemical one, is shown. The projections onto the *ab* plane are shown for magnetic moments of atoms in the chemical cell only.

the model described above with constraints implied by the symmetry of the point group C_2 (see Fig. 5). This model has already been used above in calculations of the temperature dependencies of the susceptibility, magnetic moments, and the energy spectra of the Ho^{3+} ions in the *easy-plane* phase of $HoFe_3(BO_3)_4$.

To satisfy the constraints implied by the local symmetry, a superposition of two basis functions (modes) of the two-dimensional IR *mA*3(2) should be used to describe the magnetic structure with main spin components either along the *a* axis or perpendicular to it (along the b^* axis). This means that in refinement, one has to take into consideration all atoms in the chemical cell, namely three atoms of Ho and nine atoms of Fe (three for the Fe1 site and six for the Fe2 one).

We should note also an indeterminacy of the orientation of the Fe spin in the basal plane which has been already discussed for $NdFe_3(BO_3)_4$ [45], $Nd(Tb)Fe_3(BO_3)_4$ [49], and $CeFe_3(BO_3)_4$ [50]. Such a situation is caused by a very small anisotropy within the basal plane, which results in a multidomain structure when all orientations of the spin in the basal plane are equally probable. To take into account this degeneracy the three-domain approach should be considered as an adequate model and it was used in the refinement.

Taking these constraints into account and using the three-domain approach for Fe spins, the refinement demonstrates a magnetic structure with out-of-plane components of the Ho moments [Fig. 7(b)]. The goodness-of-fit of this model which suggests collinear Fe1 and Fe2 magnetic moments aligned along the *a* axis goes down to 1.98 ($R_{obs} = 10.3$) against 2.31 ($R_{obs} = 13.5$) calculated for the model with out-of-plane components of the Fe2 moments and the Ho moments within the *ab* plane, suggested from neutron powder diffraction [18]. The model with the Fe moments within the *ab* plane and out-of-plane components of the Ho moments is supported not only by the observed goodness-of-fit factors but also by the following physical arguments.

The physical reason for a noncollinear arrangement of the Ho moments with a noticeable component along the *c* axis is an anisotropic holmium susceptibility tensor with off-diagonal components, which is a consequence of the C_2 local symmetry of holmium sites in the space group $P3_121$. An additional argument for a collinear model of the Fe magnetic structure is that it is determined by a strong isotropic Fe-Fe exchange and was already confirmed for the isostructural $YFe_3(BO_3)_4$ in Ref. [39]. Note that the *easy-plane* magnetic structure with significant out-of-plane Fe2 components proposed for $HoFe_3(BO_3)_4$ in Ref. [18] looks surprising and unexpected and it would require special relations for the Fe-Fe exchange parameters. The refinement quality with observed and calculated square of the structure factors F^2 is shown in Fig. 8. Table IV presents the refined values of moments and angles in this model.

It should be noted that the refinement gives estimations for the deviation angles from the *a* axis in the *ab* plane and from the *c* axis for the Ho2 (Ho3) moments (Table IV), which agree qualitatively with corresponding angles at 7 K obtained from calculations, namely, $\varphi \approx \pm 167^\circ$ and $\theta \approx 48^\circ$ (132°) (see Sec. IV B).

TABLE III. Magnetic moments *M* (in Bohr magnetons) and their orientation in the easy-axis magnetic structure in $HoFe_3(BO_3)_4$ at 1.6 K (φ is the angle in the *ab* plane relative to the *a* axis, θ is the deviation from the *c* axis). In the brackets, errors [estimated standard deviations (e.s.d.)] are given.

	M (μ_B)	φ (degrees)	θ (degrees)
Ho1	5.2(1)	−30.0	−38(2)
Ho2	5.2(1)	30.0	−142(2)
Ho3	5.2(1)	−90.0	142(2)
Fe1	3.5(1)	150.0 or −30.0	5(3) or 175(3)
Fe2	3.5(1)	−150.0 or 30.0	6(2) or −174(2)

C. Spin-reorientation transition

Figure 9 shows the temperature dependencies of the intensities of two characteristic reflections, 0 0 3/2 and 0 0 1/2. The reflection 0 0 3/2 exists in the *easy-plane* state only; at the spin-reorientation transition it disappears. For the 0 0 1/2 reflection, the opposite is true, it disappears above the

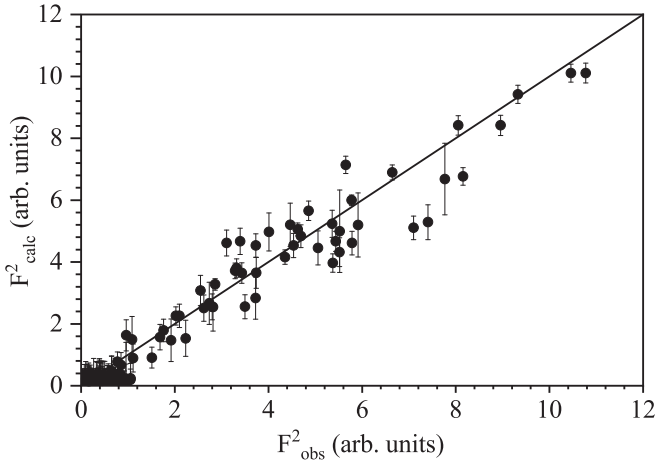

FIG. 8. Results of refinement of the *easy-plane* state at 7 K. There are 199 nonequivalent reflections in the refinement.

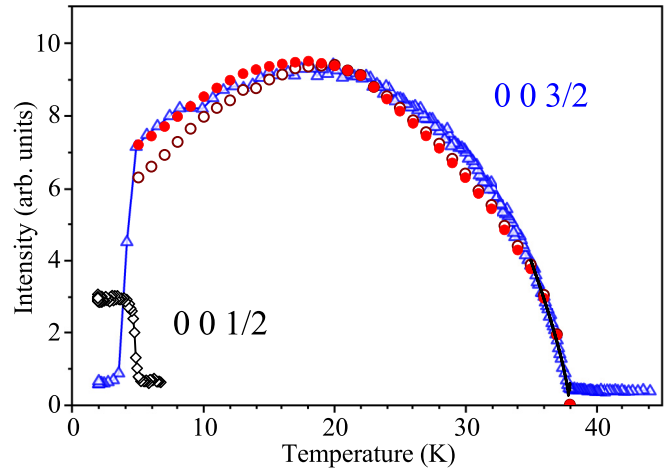

FIG. 9. Measured and calculated intensities vs temperature of the two characteristic reflections 0 0 1/2 and 0 0 3/2. The measured intensities are shown in black diamonds and blue triangles, respectively. The calculated intensity for the model with Fe moments within a basal plane and the model with out-of-plane Fe moments [18] are shown in red closed circles and brown open circles, respectively. The fit near T_N by the dependence $I \sim (1 - T/T_N)^{2\beta}$ with $T_N = 37.88(2)$ K and $\beta = 0.45(3)$ is shown in a black line.

transition. The fitting of the temperature dependence of the integral intensity of the reflection peak 0 0 3/2 near the magnetic transition by a power law $(1 - T/T_N)^{2\beta}$, shown in Fig. 9, indicates the Néel temperature of 37.88(2) K and a critical exponent $\beta = 0.45(3)$. The latter is close to 0.5—the critical exponent in the mean-field approximation.

Figure 9 demonstrates a decrease of the intensity of the 0 0 3/2 peak below the temperature of about 20 K. To find the reason for this drop in intensity, we have modeled the intensity of this peak; it depends on the M_a components of the magnetic moments [see Eqs. (S10) and (S11) in the Supplemental Material [27]]. Based on the magnetic structure proposed in Sec. IV (with Fe spins within the *ab* plane and out-of-plane components of the Ho moments) and using the calculated projections of the holmium magnetic moments on the *a* axis in the easy-plane phase presented in Sec. IV B (in particular, in Fig. 6) and the iron magnetic moments in the magnetically ordered easy-plane phase of $YFe_3(BO_3)_4$ [39], we obtained the temperature dependence of the 0 0 3/2 reflection intensity shown in Fig. 9 (see the Supplemental Material [27] for details).

The calculated curve reproduces well the experimental data. The analysis shows that the reason for the low-temperature drop in intensity lies in the rotation of the Ho2 (Ho3) moments towards the collinear structure and strongly different temperature dependencies of the spontaneous Fe and induced Ho magnetic moments.

TABLE IV. Magnetic moments and their orientation in the *easy-plane* magnetic structure in $HoFe_3(BO_3)_4$ at 7 K. φ is the angle in the *ab* plane relative to the *a* axis, θ is the deviation from the *c* axis. In the brackets, errors [estimated standard deviations (e.s.d.)] are given.

	M (μ_B)	φ (degrees)	θ (degrees)
Ho1	4.19(1)	0	90
Ho2	4.19(1)	150(2)	77(2)
Ho3	4.19(1)	−150(2)	103(2)
Fe1 (3 *a*), Fe2 (6 *c*)	3.56(1)	0 or 180	90

We also calculated the discussed dependence for the model proposed in Ref. [18] (with out-of-plane components of Fe spins and Ho moments within the *ab* plane). This curve also presented in Fig. 9 demonstrates poorer agreement with the experiment below about 20 K, which is an additional argument in favor of our model.

D. Refinement in the magnetic field

To obtain a ferromagnetic moment due to the canting of the antiferromagnetic structure in the applied magnetic field, the polarized neutron technique known as the "flipping ratio" was used. In this method, all nuclear reflections are measured with the polarization of the incident neutrons "up" or "down" relative to the applied magnetic field [51].

In the applied magnetic field, a net ferromagnetic moment appears, which contributes to the nuclear reflections. In Fig. 10, such contribution vs the applied magnetic field is shown for two characteristic reflections 1 4 0 and 0 0 6. In magnetic diffraction, only the moment projection, which is perpendicular to the diffraction vector, is measured. Therefore, from Fig. 10 it is seen that a net ferromagnetic moment appears both in the *ab* plane (reflection 0 0 6) and along the *c* axis (reflection 1 4 0), although the magnetic field was applied in the *ab* plane along the *a* axis. This confirms the existence of off-diagonal terms in the susceptibility tensor.

From the flipping ratio data, ferromagnetic components along the *a* axis were refined, using the flipping ratio option implemented in the FULLPROOF Suite Package [52]. They are plotted in Fig. 11 vs the applied magnetic field for Ho and Fe1 and Fe2 ions. It can be seen that the magnetic susceptibility of the Fe subsystem is negligible compared to the susceptibility of the Ho subsystem.

The antiferromagnetic structure refined from the antiferromagnetic reflections measured in different applied magnetic

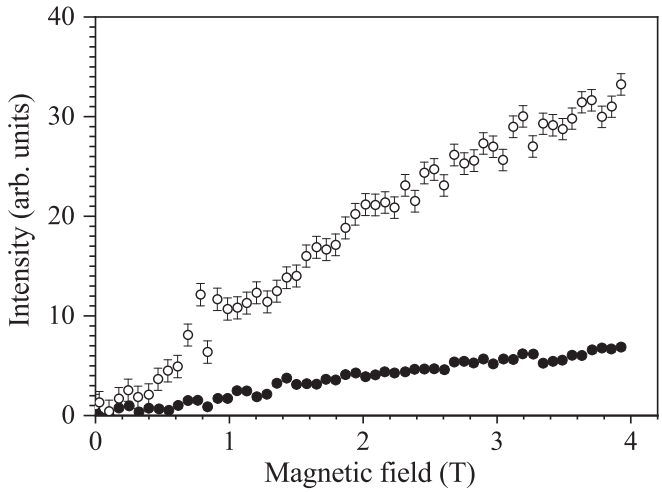

FIG. 10. The magnetic contribution to the intensities of the nuclear reflections 0 0 6 (open circles) and 1 4 0 (closed circles), due to the projections of a net ferromagnetic moment onto the *ab* plane and the *c* axis, respectively, vs the applied magnetic field $\boldsymbol{B} \parallel a$ at $T = 1.7$ K. At $B < B_{\rm crit} \approx 0.9$ T $HoFe_3(BO_3)_4$ is in the *easy-axis* phase but at $B > B_{\rm crit}$ it is in the *easy-plane* phase [19].

fields $B > B_{\rm crit} \approx 0.9$ T appeared to be of the *easy-plane* type, in accordance with Ref. [19]. The only difference with the structure refined in the zero field is the reduced components of the antiferromagnetic moment. The ferromagnetic component of the total moment (Fig. 11) contributes to the nuclear reflections, while the antiferromagnetic component contributes to the antiferromagnetic reflections. Because the total moment remains constant, the antiferromagnetic component reduces.

In summary, the results of the single-crystal neutron diffraction confirm the proposed model of the easy-plane magnetic structure with the Fe spins within the basal plane and out-of-plane components of the Ho moments.

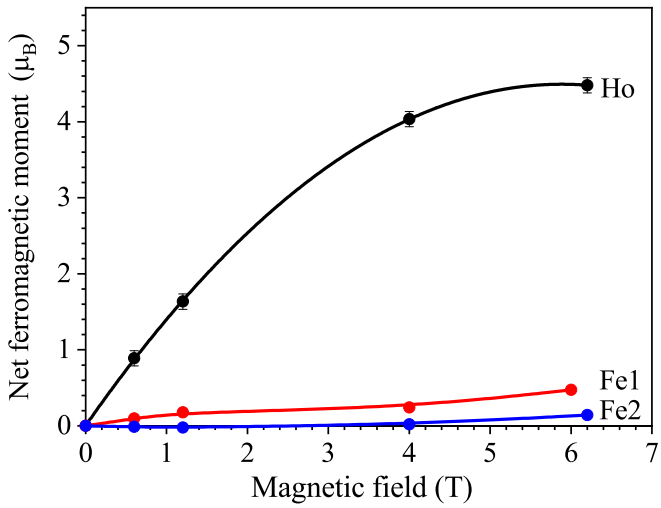

FIG. 11. The net ferromagnetic moments along the *a* axis vs the applied magnetic field $\boldsymbol{B} \parallel a$ for Ho (black), Fe1 (red), and Fe2 (blue) ions obtained with the flipping ratio method. An error is a symbol size. $T = 1.7$ K.

VI. CONCLUSIONS

The presented investigation, on the example of a multiferroic holmium iron borate, shows the fruitfulness of the combined approach to determining the magnetic structure of complex multisublattice magnets. This approach includes measurements using neutron diffraction and high-resolution optical spectroscopy, as well as in-depth theoretical analysis based on physically grounded models.

We have performed the high-resolution spectroscopic and elastic neutron scattering studies of holmium iron borate $HoFe_3(BO_3)_4$ single crystals in the temperature range 1.7–150 K that covers both the paramagnetic phase ($T > T_N = 38.5$ K) and two magnetic phases, the *easy-plane* ($T_N > T > T_{SR}$) and the *easy-axis* ($T < T_{SR}$) ones. Below ~360 K, i.e., in the whole temperature range studied, the crystal structure of $HoFe_3(BO_3)_4$ is described by the $P3_121$ trigonal space symmetry group. What is important, in this space group, is that the symmetry of the Ho site is low (C_2) and there are two nonequivalent positions for Fe atoms, Fe1 and F2, in contrast to the case of the parent $R32$ structure where Ho^{3+} resides in the D_3 symmetry positions and only one Fe site exists.

The analysis of high-resolution spectroscopy data in all three magnetic phases revealed a complete scheme of the $4f$ energy levels of the Ho^{3+} ions up to 24 000 cm^{-1}. This set of data was used to derive the crystal-field model (starting from the initial set of crystal-field parameters obtained in the framework of the exchange-charge model) as well as to evaluate the exchange-interaction parameters. Such approach delivered a set of physically reasonable CF and EI parameters. These data were further used to calculate the magnetic susceptibilities of the Ho subsystem and of $HoFe_3(BO_3)_4$, based on the results obtained earlier for the Fe chains in RE and yttrium iron borates and on the model of the magnetic structure in the *easy-plane* phase that followed from these results.

The main result of this theoretical consideration is that, in the *easy-plane* magnetic phase, due to the C_2 local symmetry of the Ho sites and, as a consequence, a presence of the off-diagonal terms in the magnetic susceptibility tensor of the Ho ions, Ho^{3+} moments possess a noticeable component along the trigonal *c* axis.

The thus obtained model of the *easy-plane* magnetic structure was used in the refinement of the single-crystal neutron scattering data collected in the present study. The observed goodness-of-fit factors confirm the model with the Fe moments within the *ab* plane and out-of-plane components of the Ho moments. The results of the flipping ratio neutron technique applied to the study of $HoFe_3(BO_3)_4$ in an external magnetic field confirm the existence of off-diagonal terms in the susceptibility tensor and clearly show that the magnetic susceptibility of the Fe subsystem is negligible compared to the susceptibility of the Ho subsystem. Both the single-crystal neutron scattering data and the theoretical analysis reveal a rotation of the Ho^{3+} moments towards a collinear structure at temperatures below ~20 K.

An important conclusion that follows from our thorough study of $HoFe_3(BO_3)_4$ by different methods, including a comprehensive theoretical consideration, as well as from previous studies of Tb, Er, and Dy iron borates [37,38,42], is that the observed specific features of the magnetic susceptibilities and the magnetic structures of RE iron borates in the $P3_121$

TABLE V. Crystal-field levels of a non-Kramers RE ion placed into the D_3 and C_2 symmetry positions of a crystal. J is the total momentum characterizing an energy level of a free ion. $\Gamma_1(\gamma_1)$ and $\Gamma_2(\gamma_2)$ are one-dimensional representations but Γ_3 is a two-dimensional one.

	D_3		C_2	
J	Irreducible representations	Number of levels	Irreducible representations	Number of levels
0	Γ_1	1	γ_1	1
1	$\Gamma_2+\Gamma_3$	2	$\gamma_1+2\gamma_2$	3
2	$\Gamma_1+2\Gamma_3$	3	$3\gamma_1+2\gamma_2$	5
3	$\Gamma_1+2\Gamma_2+2\Gamma_3$	5	$3\gamma_1+4\gamma_2$	7
4	$2\Gamma_1+\Gamma_2+3\Gamma_3$	6	$5\gamma_1+4\gamma_2$	9
5	$\Gamma_1+2\Gamma_2+4\Gamma_3$	7	$5\gamma_1+6\gamma_2$	11
6	$3\Gamma_1+2\Gamma_2+4\Gamma_3$	9	$7\gamma_1+6\gamma_2$	13
7	$2\Gamma_1+3\Gamma_2+5\Gamma_3$	10	$7\gamma_1+8\gamma_2$	15
8	$3\Gamma_1+2\Gamma_2+6\Gamma_3$	11	$9\gamma_1+8\gamma_2$	17

structural phase are defined, essentially, by the energy patterns of the ground multiplet and symmetry properties of the wave functions of the lower CF energy levels of a RE ion in the crystal field of the C_2 symmetry.

ACKNOWLEDGMENTS

Financial support of the Russian Science Foundation under Grant No. 19-12-00413 is acknowledged. I.V.G. acknowledges financial support of the neutron scattering studies from the Russian Foundation for Basic Research under Grant No. 20-02-00109. The analysis of the measured neutron diffraction data was performed by A.A.M. with support of the Russian Science Foundation under Grant No. 16-12-10531.

APPENDIX A: CRYSTAL-FIELD SPLITTING AND OPTICAL SELECTION RULES FOR THE D_3 AND C_2 POINT SYMMETRY GROUPS

The Stark structure of J multiplets and selection rules for optical transitions in the crystal fields with the D_3 and C_2 symmetry are presented in Tables V and VI, respectively.

APPENDIX B: MAGNETIC SUSCEPTIBILITY OF $HoFe_3(BO_3)_4$

1. Anisotropic Fe-Ho exchange interaction in the mean-field approximation

1.1. Easy-plane phase

The Hamiltonian $H_{\rm exch}({\rm Ho}k)$ describes the interaction of holmium ions in the sixfold iron coordination with exchange fields at the corresponding sites ($k=1$ and $k=2$), in the mean-field approximation:

$$H_{\rm exch}({\rm Ho1}) = 6J_{fd,x}M_{\rm Fe}(T)S_{{\rm Ho},x}/\mu_B, \tag{B1}$$

$$H_{\rm exch}({\rm Ho2, Ho3}) = 6M_{\rm Fe}(T)\left(-\frac{1}{2}J_{fd,x}S_{{\rm Ho},x} \pm \frac{\sqrt{3}}{2}J_{fd,y}S_{{\rm Ho},y}\right)\Big/\mu_B. \tag{B2}$$

1.2. Easy-axis phase

Below the spin-reorientation temperature $T_{\rm SR}$, when the iron magnetic moments $M_{{\rm Fe},z}$ are parallel to the c axis [18], the exchange Hamiltonian reads ($k=1$–3)

$$H_{\rm exch}({\rm Ho}k) = 6J_{fd,z}M_{{\rm Fe},z}(T)S_{{\rm Ho},z}/\mu_B. \tag{B3}$$

All holmium ions are equivalent.

2. Holmium susceptibilities in the magnetically ordered phases

In the magnetically ordered phases, the holmium susceptibilities, which determine additional magnetic moments induced by the external magnetic field $\boldsymbol{B}$, are computed directly in the local Cartesian systems of coordinates using the expression $\chi_{{\rm Ho}k,\alpha\beta}(T<T_{\rm N}) = \Delta M_\alpha({\rm Ho}k, B_\beta)/B_\beta$, $B_\beta = 0.1$ T, where

$$\Delta M_\alpha({\rm Ho}k, T, B_\beta) = \frac{{\rm Tr}\{m_\alpha \exp[-H_{\rm eff}({\rm Ho}k, B_\beta)/k_BT]\}}{{\rm Tr}\{\exp[-H_{\rm eff}({\rm Ho}k, B_\beta)/k_BT]\}} - M_\alpha({\rm Ho}k, T) \tag{B4}$$

TABLE VI. Selection rules for the electric dipole (ED) and magnetic dipole (MD) transitions of a non-Kramers ion in the D_3 and C_2 positions. The axes *x, y, z* of a local Cartesian system of coordinates are oriented relative to the crystal axes *a, b, c* in the following way: $z \parallel c$, $x \parallel a \parallel C_2$, $y \perp a$. Allowed components of the ED (MD) moment are denoted as d_i (μ_i), $i = x,\ y,\ z$.

	ED			MD		
$\boldsymbol{D_3}$	Γ_1	Γ_2	Γ_3	Γ_1	Γ_2	Γ_3
Γ_1		d_z π	$d_x,\ d_y$ α, σ		μ_z σ	$\mu_x,\ \mu_y$ α, π
Γ_2	d_z π		$d_x,\ d_y$ α, σ	μ_z σ		$\mu_x,\ \mu_y$ α, π
Γ_3	$d_x,\ d_y$ α, σ	$d_x,\ d_y$ α, σ	$d_x,\ d_y,\ d_z$ α, σ, π	$\mu_x,\ \mu_y$ α, π	$\mu_x,\ \mu_y$ α, π	$\mu_x,\ \mu_y,\ \mu_z$ α, σ, π
$\boldsymbol{C_2}$	γ_1	γ_2		γ_1	γ_2	
γ_1	d_x α, σ	$d_z,\ d_y$ α, σ, π		μ_x α, π	$\mu_z,\ \mu_y$ α, σ, π	
γ_2	$d_z,\ d_y$ α, σ, π	d_x α, σ		$\mu_z,\ \mu_y$ α, σ, π	μ_x α, π	

and

$$H_{\rm eff}({\rm Ho}k, B_\beta) = H_{\rm FI} + H_{\rm CF} + H_{\rm exch}({\rm Ho}k) - m_\beta B_\beta. \tag{B5}$$

$H_{\rm exch}({\rm Ho}k)$ is determined by Eqs. (B1)–(B3).

[1] H. Schmid, Introduction to the proceedings of the 2nd international conference on magnetoelectric interaction phenomena in crystals, MEIPIC-2, Ferroelectrics **161**, 1 (1994).

[2] N. A. Spaldin and M. Fiebig, The renaissance of magnetoelectric multiferroics, Science **309**, 391 (2005).

[3] S.-W. Cheong and M. Mostovoy, Multiferroics: a magnetic twist for ferroelectricity, Nat. Mater. **6**, 13 (2007).

[4] Y. Tokura, S. Seki, and N. Nagaosa, Multiferroics of spin origin, Rep. Prog. Phys. **77**, 076501 (2014).

[5] S. Dong, J.-M. Liu, S.-W. Cheong, and Z. Ren, Multiferroic materials and magnetoelectric physics: symmetry, entanglement, excitation, and topology, Adv. Phys. **64**, 519 (2015).

[6] A. M. Kadomtseva, Y. F. Popov, G. P. Vorob'ev, A. P. Pyatakov, S. S. Krotov, K. I. Kamilov, V. Y. Ivanov, A. A. Mukhin, A. K. Zvezdin, A. M. Kuz'menko, L. N. Bezmaternykh, I. A. Gudim, and V. L. Temerov, Magnetoelectric and magnetoelastic properties of rare-earth ferroborates, Low Temp. Phys. **36**, 511 (2010) [Fiz. Nizk. Temp. **36**, 640 (2010)].

[7] Y. A. Izyumov, V. E. Naish, and R. P. Ozerov, *Neutron Diffraction of Magnetic Materials* (Consultants Bureau, New York, 1991).

[8] *Neutron Scattering from Magnetic Materials*, edited by T. Chatterji (Elsevier, 2006).

[9] Z. Wang, N. Qureshi, S. Yasin, A. Mukhin, E. Ressouche, S. Zherlitsyn, Y. Skourski, J. Geshev, V. Ivanov, M. Gospodinov, and V. Skumryev, Magnetoelectric effect and phase transitions in CuO in external magnetic fields, Nat. Commun. **7**, 10295 (2016).

[10] I. Urcelay-Olabarria, E. Ressouche, Z. Wang, Y. Skourski, V. Y. Ivanov, Y. F. Popov, G. P. Vorobev, A. M. Balbashov, N. Qureshi, J. L. García-Muñoz, V. Skumryev, and A. A. Mukhin, Magnetic field-induced phase transitions and phase diagrams of multiferroic $Mn_{0.95}Co_{0.05}WO_4$ with cycloidal spin structure. Phys. Rev. B **96**, 104435 (2017).

[11] P. Yanda, I. V. Golosovsky, I. Mirebeau, N. V. Ter-Oganessian, J. Rodriguez-Carvajal, and A. Sundaresan, Interplay of 4 f -3 d interactions and spin-induced ferroelectricity in the green phase Gd_2BaCuO_5, Phys. Rev. Res. **2**, 023271 (2020).

[12] C.-K Loong and L Soderholm, Rare earth crystal field spectroscopy by neutron magnetic scattering: from xenotime to high T_c superconductors, J. Alloys Compd. **207-208**, 153 (1994).

[13] N. I. Leonyuk and L. I. Leonyuk, Growth and characterization of $RM_3(BO_3)_4$ crystals, Prog. Cryst. Growth Charact. **31**, 179 (1995).

[14] S. A. Klimin, D. Fausti, A. Meetsma, L. N. Bezmaternykh, P. H. M. van Loosdrecht, and T. T. M. Palstra, X-ray structure determination of the trigonal iron-helicoidal-chain compound $GdFe_3(BO_3)_4$, Acta Crystallogr., Sect. B: Struct. Sci. **61**, 481 (2005).

[15] M. N. Popova, Optical spectroscopy of low-dimensional rare-earth iron borates, J. Magn. Magn. Mater. **321**, 716 (2009).

[16] R. P. Chaudhury, F. Yen, B. Lorenz, Y. Y. Sun, L. N. Bezmaternykh, V. L. Temerov, and C. W. Chu, Magnetoelectric effect and spontaneous polarization in $HoFe_3(BO_3)_4$ and $Ho_{0.5}Nd_{0.5}Fe_3(BO_3)_4$, Phys. Rev. B **80**, 104424 (2009).

[17] T. N. Stanislavchuk, E. P. Chukalina, M. N. Popova, L. N. Bezmaternykh, and I. A. Gudim, Investigation of the iron borates $DyFe_3(BO_3)_4$ and $HoFe_3(BO_3)_4$ by the method of Er^{3+} spectroscopic probe, Phys. Lett. A. **368**, 408 (2007).

[18] C. Ritter, A. Vorotynov, A. Pankrats, G. Petrakovskii, V. Temerov, I. Gudim, and R. Szymczak, Magnetic structure in iron borates $RFe_3(BO_3)_4$ (R= Y, Ho): a neutron diffraction and magnetization study, J. Phys.: Condens. Matter **20**, 365209 (2008).

[19] A. Pankrats, G. Petrakovskii, A. Kartashev, E. Eremin, and V. Temerov, Low-temperature magnetic phase diagram of $HoFe_3(BO_3)_4$ holmium ferroborate: a magnetic and heat capacity study, J. Phys.: Condens. Matter **21**, 436001 (2009).

[20] D. A. Erofeev, E. P. Chukalina, M. N. Popova, L. N. Bezmaternykh, and I. A. Gudim, High-resolution spectroscopy of $HoFe_3(BO_3)_4$ crystal: A study of phase transitions, Opt. Spectrosc. **120**, 558 (2016) [Opt. Spektrosk. **120**, 588 (2016)].

[21] D. K. Shukla, S. Francoual, A. Skaugen, M. v. Zimmermann, H. C. Walker, L. N. Bezmaternykh, I. A. Gudim, V. L. Temerov, and J. Strempfer, Ho and Fe magnetic ordering in multiferroic $HoFe_3(BO_3)_4$, Phys. Rev. B **86**, 224421 (2012).

[22] A. I. Popov, D. I. Plokhov, and A. K. Zvezdin, Quantum theory of magnetoelectricity in rare-earth multiferroics: Nd, Sm, and Eu ferroborates, Phys. Rev. B **87**, 024413 (2013).

[23] N. V. Kostyuchenko, A. I. Popov, and A. K. Zvezdin, Features of magnetic and magnetoelectric properties of rare-earth multiferroic $PrFe_3(BO_3)_4$ with the singlet ground state, Phys. Solid State **54**, 1591 (2012) [Fiz. Tverd. Tela **54**, 1493 (2012)].

[24] I. A. Gudim, E. V. Eremin, and V. L. Temerov, Flux growth and spin reorientation in trigonal $Nd_{1-x}Dy_xFe_3(BO_3)_4$ single crystals, J. Crystal Growth **312**, 2427 (2010).

[25] A. V. Malakhovskii, S. L. Gnatchenko, I. S. Kachur, V. G. Piryatinskaya, and I. A. Gudim, Low-temperature absorption spectra and electron structure of $HoFe_3(BO_3)_4$ single crystal, Low Temp. Phys. **43**, 610 (2017) [Fiz. Nizk. Temp. **43**, 764 (2017)].

[26] A. M. Kalashnikova, V. V. Pavlov, R. V. Pisarev, L. N. Bezmaternykh, M. Bayer, and T. Rasing, Linear and nonlinear optical spectroscopy of gadolinium iron borate $GdFe_3(BO_3)_4$, JETP Lett. **80**, 293 (2004) [Pis'ma Zh. Eksp. Teor. Fiz. **80**, 339 (2004)].

[27] See Supplemental Material at http://link.aps.org/supplemental/10.1103/PhysRevB.103.094411 for (1) the complete table of energies of the crystal-field levels of Ho^{3+} in $HoFe_3(BO_3)_4$; (2) parameters of the effective Hamiltonian (with additional references [53–55]); (3) shifts of the CF energy levels in magnetically ordered phases; (4) details of calculation of

the temperature dependence of the intensity of the neutron-scattering reflection 0 0 3/2.

[28] A. Baraldi, R. Capelletti, M. Mazzera, N. Magnani, I. Földvári, and E. Beregi, Hyperfine interaction ns in YAB:Ho^{3+}: A high-resolution spectroscopy investigation, Phys. Rev. B **76**, 165130 (2007).

[29] A. V. Malakhovskii, S. L. Gnatchenko, I. S. Kachur, V. G. Piryatinskaya, and I. A. Gudim, Transformation of the $HoFe_3(BO_3)_4$ absorption spectra at reorientation magnetic transitions and local properties in the excited $^5F_5$ states of the Ho^{3+} ion, Phys. Rev. B **96**, 224430 (2017).

[30] A. V. Malakhovskii, S. L. Gnatchenko, I. S. Kachur, V. G. Piryatinskaya, and I. A. Gudim, Magnetic field induced local structural transformations in the optically excited states $^5F_2$ and $^5F_3$ of $HoFe_3(BO_3)_4$ single crystal, J. Magn. Magn. Mater. **476**, 177 (2019).

[31] A. V. Malakhovskii, V. V. Sokolov, I. A. Gudim, and M. V. Rautskii, Magnetic circular dichroism and absorption spectra of $^5I_8 \rightarrow {}^5F_5$ transition in $HoAl_3(BO_3)_4$ and $HoFe_3(BO_3)_4$ single crystals, Phys. Lett. A **383**, 1960 (2019); A. V. Malakhovskii, V. V. Sokolov, and I. A. Gudim, Magnetic circular dichroism and $f-f$ transitions $^5I_8 \rightarrow {}^5F_2$ and $^5F_3$ in the $HoFe_3(BO_3)_4$ single crystal, Low Temp. Phys. **46**, 734 (2020) [Fiz. Nizk. Temp. **46**, 869 (2020)].

[32] A. A. Demidov and D. V. Volkov, Magnetic properties of $HoFe_3(BO_3)_4$, Phys. Solid State **53**, 985 (2011) [Fiz. Tverd. Tela **53**, 926 (2011)].

[33] M. N. Popova, T. N. Stanislavchuk, B. Z. Malkin, and L. N. Bezmaternykh, Breaking of the Selection Rules for Optical Transitions in the Dielectric $PrFe_3(BO_3)_4$ Crystal by the Praseodymium-Iron Exchange Interaction, Phys. Rev. Lett. **102**, 187403 (2009).

[34] B. Z. Malkin, Crystal field and electron-phonon interaction in rare-earth ionic paramagnets, in *Spectroscopy of Solids Contaning Rare Earth Ions*, edited by A. A. Kaplyanskii and R. M. Macfarlane (North-Holland, Amsterdam, 1987), Chap. 2, pp. 13–50.

[35] M. N. Popova, E. P. Chukalina, B. Z. Malkin, D. A. Erofeev, L. N. Bezmaternykh, and I. A. Gudim, Crystal field and exchange interactions in the $SmFe_3(BO_3)_4$ multiferroic, JETP **118**, 111 (2014) [Zh. Exp. Teor. Fiz. **145**, 128 (2014)].

[36] M. N. Popova, T. N. Stanislavchuk, B. Z. Malkin, and L. N. Bezmaternykh, Optical spectroscopy of $PrFe_3(BO_3)_4$: Crystal-field and anisotropic Pr-Fe exchange interactions, Phys. Rev. B **80**, 195101 (2009).

[37] M. N. Popova, T. N. Stanislavchuk, B. Z. Malkin, and L. N. Bezmaternykh, Phase transitions and crystal-field and exchange interactions in $TbFe_3(BO_3)_4$ as seen via optical spectroscopy, J. Phys.: Condens. Matter **24**, 196002 (2012).

[38] M. N. Popova, E. P. Chukalina, D. S. Erofeev, A. Jablunovskis, I. A. Gudim, and B. Z. Malkin, High-resolution optical spectroscopy and modeling of spectral and magnetic properties of multiferroic $ErFe_3(BO_3)_4$, Phys. Rev. B **101**, 205108 (2020).

[39] B. Z. Malkin, E. A. Popova, E. P. Chukalina, A. Jablunovskis, and M. N. Popova, Self-consistent four-particle cluster model of Fe^{3+} Heisenberg chains: Spectral and magnetic properties of $YFe_3(BO_3)_4$ crystals, Phys. Status Solidi RRL **14**, 1900603 (2020).

[40] W. T. Carnall, G. L. Goodman, K. Rajnak, and R. S. Rana, A systematic analysis of the spectra of the lanthanides doped into single crystal LaF_3, J. Chem. Phys. **90**, 3443 (1989).

[41] E. S. Smirnova, O. A. Alekseeva, A. P. Dudka, D. N. Khmelenin, K. V. Frolov, M. V. Lyubutina, I. A. Gudim, and I. S. Lyubutin, Crystal structure and structural phase transition in bismuth-containing $HoFe_3(BO_3)_4$ in the temperature range 11–500 K, Acta Crystallogr., Sect. B **75**, 954 (2019).

[42] M. N. Popova, E. P. Chukalina, K. N. Boldyrev, T. N. Stanislavchuk, B. Z. Malkin, and I. A. Gudim, Spectroscopy of f-f transitions, crystal-field calculations, and magnetic and quadrupole helix chirality in $DyFe_3(BO_3)_4$, Phys. Rev. B **95**, 125131 (2017).

[43] M. N. Popova, B. Z. Malkin, K. N. Boldyrev, T. N. Stanislavchuk, D. A. Erofeev, V. L. Temerov, and I. A. Gudim, Evidence for a collinear easy-plane magnetic structure of multiferroic $EuFe_3(BO_3)_4$: Spectroscopic and theoretical studies, Phys. Rev. B **94**, 184418 (2016).

[44] I. V. Golosovsky, A. K. Ovsyanikov, D. N. Aristov, P.G. Matveeva, A. A. Mukhun, M. Boehm, L.-P. Regnault, and L. N. Bezmaternykh, Spin-wave dynamics and exchange interactions in $NdFe_3(BO_3)_4$ explored by inelastic neutron scatteting, J. Magn. Magn. Mater. **451**. 443 (2018).

[45] M. Janoschek, P. Fischer, J. Schefer, B. Roessli, V. Pomjakushin, M. Meven, V. Petricek, G. Petrakovskii, and L. Bezmaternikh, Single magnetic chirality in the magnetoelectric $NdFe_3(^{11}BO_3)_4$, Phys. Rev. B **81**, 094429 (2010).

[46] A. M. Kadomtseva, G. P. Vorob'ev, Y. F. Popov, A. P. Pyatakov, A. A. Mukhin, V. Y. Ivanov, A. K. Zvezdin, I. A. Gudim, V. L. Temerov, and L. N. Bezmaternykh, Magnetoelectric and magnetoelastic properties of easy-plane ferroborates with a small ionic radius, JETP **114**, 810 (2012) [Zh. Eksp. Teor. Fiz. **141**, 930 (2012)].

[47] http://jana.fzu.cz.

[48] Bilbao Crystallographic Server, https://www.cryst.ehu.es.

[49] I. V. Golosovsky, A. I. Vasilev, A. A. Mukhin, E. Ressouche, V. Skumryev, I. Urcelay-Olabarria, I. A. Gudim, and L. N. Bezmaternykh, Complex magnetic order in the $Nd(Tb)Fe_3(BO_3)_4$ multiferroic revealed by single-crystal neutron diffraction, Phys. Rev. B **99**, 134439 (2019).

[50] S. Hayashida, S. Asai, D. Kato, S. Hasegawa, M. Avdeev, H. Cao, and T. Masuda, Magnetic order in the rare-earth ferroborate $CeFe_3(BO_3)_4$, Phys. Rev. B **98**, 224405 (2018).

[51] B. Gillon, The classical flipping ratio technique applied to non classical magnetic materials: Molecule-based and photoswitchable magnetic compounds, Collection SFN **7**, 13 (2007).

[52] C. Frontera and J. Rodríguez-Carvajal, FullProf as a new tool for flipping ratio analysis:further improvements, Physica B **350**, e-731 (2004).

[53] R. P. Gupta and S. K. Sen, Sternheimer shielding-antishielding; Rare-Earth ions, Phys. Rev. A **7**, 850 (1973).

[54] O. J. Sovers, Trivalent lanthanide 4f electron radial wave functions, J. Phys. Chem. Solids **28**, 1073 (1967).

[55] E. Clementi and A. D. McLean, Atomic negative ions, Phys. Rev. **133**, A419 (1964).